Internal structure of the Paleoarchean Mt Edgar dome, Pilbara Craton, Western Australia

Nicolas M. Roberts and Basil Tikoff

Abstract

The Paleoarchean East Pilbara Terrane of Western Australia is a dome-and-keel terrane that is often highlighted as recording a vertically convective tectonic regime in the early Earth. In this model, termed 'partial convective overturn', granitic domes diapirically rose through a dense, foundering mafic supracrustal sequence. The applicability of partial convective overturn to the East Pilbara Terrane and to other Archean dome-and-keel terranes is widely debated and has significant implications for early Earth geodynamics. A critical data gap in the East Pilbara Terrane is the internal structure of the granitic domes. We present field-based, microstructural, and anisotropy of magnetic susceptibility (AMS) data collected within the Mt Edgar dome to understand its internal structure and assess its compatibility with existing dome formation models. Field and microstructural observations suggest that most fabric development occurred under submagmatic and high-temperature solid-state conditions. The AMS results reveal a coherent, dome-wide structural pattern: 1) Sub-vertical lineations plunge radially inward towards the center of the dome and foliations across much of the dome consistently strike northwest; 2) Shallowly plunging lineations define an arch that extends from the center of the dome to the southwest margin; and 3) Migmatitic gneisses, which represent the oldest granitic component of the dome, are folded and flattened against the margin of the dome in two distinct lobes. The structural relationships between rocks of different ages indicate that units of different crystallization ages deformed synchronously during the last major pulse of granitic magmatism.

These data are broadly consistent with a vertical tectonics model, and we synthesize our structural results to propose a three-stage diapiric evolution of the Mt Edgar dome. The critical stage of dome development was between 3.3 and 3.2 Ga, when widespread, melt-assisted flow of the deep crust led to the formation of a steep-walled, composite dome. These data suggest that diapiric processes were important for the formation of dome-and-keel terranes in the Paleoarchean.

Keywords

Paleoarchean, Structural Geology, Gneiss Dome, Anisotropy of Magnetic Susceptibility

Introduction

Many early continents are dominated by the presence of gneiss dome systems, termed 'dome-and-keel' terranes (e.g., Collins, 1989; Ramsay, 1989; Bouhallier et al., 1995; Kisters and Anhaeusser, 1995; Chardon et al., 1998; Bédard, 2006; Van Kranendonk, 2011; Polat et al., 2015; Liu and Wei, 2018; Webb et al., 2020; Zibra et al., 2020). Throughout Earth history, gneiss domes have played a critical role in stabilizing continental crust by advecting heat to the surface (Whitney et al., 2004; Whitney et al., 2013). Given the ubiquity of dome-and-keel terranes in the Archean, heat advection through doming is interpreted to have been important in early continental crustal processes. Gneiss domes may have been particularly important because of a high geothermal gradient and the potential absence of plate tectonics (Moore and Webb, 2013; Piper, 2013; Thébaud and Rey, 2013; Bédard, 2018; Piper, 2018). The protocontinents formed by dome-and-keel terranes often form the oldest core of Archean cratons, leading some to suggest that their formation enabled a transition towards steady-state cold-slab plate tectonics (e.g., Van Kranendonk et al., 2007).

The nature of gneiss dome construction in Archean dome-and-keel terranes is debated in the literature. Gneiss domes are interpreted to represent crustal convection driven by buoyancy instabilities and/or plume magmatism (e.g., Chardon et al., 1998; Collins et al., 1998; Bédard, 2003; Van Kranendonk, 2011; Wiemer et al., 2018; Webb et al., 2020; Zibra et al., 2020), alpine-style thrusting and core complex formation associated with orogenic collapse or extension (e.g., Zegers et al., 2001; Lana et al., 2010; Polat et al., 2016), or crustal scale buckling (Blewett, 2002; Harris et al., 2012). Not all dome-and-keel terranes necessarily formed by identical processes; different terranes may represent several parts of the early Earth tectonic system (Van Kranendonk, 2010; Nutman et al., 2015; Smithies et al., 2018) or may represent changing modes of crustal evolution throughout the Archean (Van Kranendonk et al., 2007). Regardless, each model for dome-and-keel development predict significantly different structures within gneiss domes and the mantling metamorphic sequence (Whitney et al., 2004; Yin, 2004). Since these models imply different crustal processes and tectonic regimes, structural investigation is an important approach for understanding the evolution of dome-and-keel terranes.

The Paleoarchean East Pilbara Terrane is a well exposed dome-and-keel terrane on the northern coast of Western Australia (e.g., Hickman, 1984; Collins, 1989, 1993; Zegers et al., 1996; Collins et al., 1998; Collins and Van Kranendonk, 1999; Zegers et al., 1999; Kloppenburg et al., 2001; Zegers and van Keken, 2001; Pawley et al., 2004; Van Kranendonk et al., 2004; Smithies et al., 2005; Hickman and Van Kranendonk, 2012; Thébaud and Rey, 2013; François et al., 2014; Wiemer et al., 2016; Gardiner et al., 2017; Johnson et al., 2017; Nijman et al., 2017; Wiemer et al., 2018). Although a consensus has emerged in the literature that the East Pilbara Terrane formed by buoyancy-driven crustal inversion operating in the early Earth (e.g., François et al., 2014; Wiemer et al., 2018), other models have also been proposed, including dome formation through core complex development and fold interference (Van Haaften and White, 1998; Kloppenburg et al., 2001; Zegers and van Keken, 2001; Blewett, 2002).

Because they have experienced little to no solid-state deformation since the Mesoarchean (Zegers et al., 1999), the gneiss domes of the East Pilbara Terrane provide a unique window into structures associated with Paleoarchean doming processes. The complexly deformed supracrustal belts ('greenstones') between domes and the sheared granitic margins of the East Pilbara gneiss domes have been well-studied, but disagreements exist over their structural evolution. Several studies have documented structures such as large-scale, refolded recumbent folds, multiple generations of foliation development and zones of vertical L-tectonites at dome triple junctions (Collins, 1989; Collins et al., 1998; Pawley et al., 2004), all structures consistent with the diapiric rise of the granitic domes (Mareschal and West, 1980; Whitney et al., 2004; Zibra et al., 2020). Other studies have documented unidirectional kinematics along dome margins, interpreted as early thrust stacks and extensional structures (Zegers et al., 1996; Van Haaften and White, 1998; Kloppenburg et al., 2001) that are more typical of alpine-style thrusting followed by core complex development (Whitney et al., 2013).

The interior structures of the East Pilbara domes should be able to distinguish between these two end member models. However, investigating these structures present a challenge; granitic dome rocks commonly appear massive and with only faint fabrics in the field. Studies that do document internal dome structures (Collins, 1989; Kloppenburg et al., 2001; Pawley et al., 2004; Van Kranendonk et al., 2004) focus on discrete areas within domes that are more strongly deformed. To date there is no quantitative documentation of three-dimensional foliation and lineation data within an entire dome in the East Pilbara terrane.

This study characterizes the internal structure of the Mt Edgar dome (Fig. 1) in the East Pilbara Terrane using anisotropy of magnetic susceptibility (AMS), field observations, and microstructural analysis. By using AMS as a fabric proxy, these data document the dome-wide structure and conditions of fabric development. Building upon existing datasets, a dome history of diapirism is interpreted.

Geologic Setting

The East Pilbara Terrane of Western Australia

The 3.53 - 2.83 Ga East Pilbara terrane is a classic granite-greenstone terrane. The prominent structure is that of 50-100 km diameter granitic domes with intervening supracrustal greenstone belts, which together comprise a dome-and-keel crustal architecture (Hickman, 1984; Van Kranendonk et al., 2007). Extensive regional geochronology (Nelson, 1999, 2001, 2005) reveals four pulses of granitic magmatism, each of which appear in multiple domes (Fig. 1 legend): The 3.47–3.42 Ga Callina and Tambina Supersuites, the 3.32–3.29 Ga Emu Pool Supersuite, the 3.45–3.23 Ga Cleland Supersuite, and the 2.89–2.83 Ga Split Rock Supersuite. The Split Rock Supersuite is everywhere undeformed and is thought to represent post-doming plutonism (Van Kranendonk, 2006). Granitic rocks are generally of tonalite-tronjdhemite-granodiorite (TTG) composition, though the composition of younger granitic rocks is more evolved, dominated by monzogranites (Bickle et al., 1992; Collins, 1993; Barley and Pickard, 1999). For the purposes of this structural study, the broad term *granitic* is used. On the basis of major and trace element trends as well as U-Pb and Hf isotope data from zircons, geochemical studies have suggested that younger granitic rocks of the East Pilbara terrane may have resulted from the recycling of the older granitic rocks (Collins, 1993; Barley and Pickard, 1999; Green et al., 2000; Smithies et al., 2003; Gardiner et al., 2017).

The supracrustal lithostratigraphy is age-correlative to the granitic supersuites, indicating a relationship between granitic magmatism and volcanism (Williams and Collins, 1990; Van Kranendonk, 2006). The total thickness of the supracrustal lithostratigraphy is 20 km, but it is estimated that in no single place did the thickness exceed 13 km (Van Kranendonk et al., 2007). The lithostratigraphy is organized into tight synformal belts between closely spaced domes and open synformal basins away from domes.

The Mt Edgar Dome

The Mt Edgar dome is located in the core of the East Pilbara terrane, with a nearly circular exposure of approximately 50 km in diameter (Fig. 1). The Mt Edgar dome includes granitic rocks belonging to each of the four Paleoarchean supersuites defined in the East Pilbara terrane, with volumetrically major components of Tambina, Emu Pool, and Cleland Supersuites. Rocks of the Tambina Supersuite formations are distributed along the southern, southwest, and western margin. Emu Pool rocks are distributed along the margins on the northern half of the dome and comprise much of the southern half of the dome. Cleland Supersuite rocks, thought to be the youngest rocks related to dome formation (Hickman, 2012), outcrop in the core of the dome. A recent active-source seismic profile shows that the Mt Edgar dome granitic rocks extend to a depth of ~15 km (Doublier et al., 2020).

Compositional boundaries were used to identify distinct granitic formations within the Mt Edgar dome. Boundaries were defined by integrating field mapping (Collins, 1989; Williams and Collins, 1990; Kloppenburg et al., 2001; Hickman, 2016) with flyover gamma-ray spectrometry (Minty et al., 2009). These remote sensing data, structures mapped by Collins (1989), and geochronology (Williams and Collins, 1990; Nelson, 1999, 2001, 2005b) provide the first-order constraints of the internal structure of the Mt Edgar dome.

Two lobes of mixed high and low potassium rocks mapped as Tambina Supersuite are seen in the potassium content map in Figure 1B. In the western lobe, the bands of high- and low-potassium rocks that trend northeast correlate to large scale upright folds and an associated shallowly to steeply dipping axial planar gneissic foliation (D3 in Collins, 1989). The lower potassium bands within the lobe are high grade gneisses that commonly have migmatitic components. These rocks have U-Pb zircon isotopic ages of 3430 ± 4 Ma (Geochronology dataset 148 in Nelson, 2001). In contrast, the higher potassium bands are tonalitic gneisses that do not display evidence for migmitization and have U-Pb zircon isotopic ages of 3313 ± 2 Ma (Geochronology dataset 561 in Nelson, 2005) and 3315 ± 5 Ma with younger discordant population yielding younger 3294 ± 5 Ma and 3271 ± 4 Ma ages (Geochronology dataset 288 in Nelson, 1999). The southern lobe of the Tambina Supersuite appears to be one large-scale isoclinal fold (Fig. 1B).

Emu Pool rocks along the southern and eastern margins of the Mt Edgar dome are low-potassium TTGs (Collins, 1993; Minty et al., 2009). Along these margins, macroscopic solid-state foliations are parallel to the granite-greenstone contact (Collins, 1989; Kloppenburg et al., 2001). The Joorina Granodiorite Formation, the most central Emu Pool Supersuite formation, has higher potassium content than other Emu Pool Supersuite formations due to abundance of alkali feldspar. The contact between the Joorina Granodiorite and other Emu Pool Supersuite formations is sharp, whereas the northern contact with the Cleland Supersuite age Bishop Creek Monzogranite Formation to the north is diffuse (Fig. 1A). The northernmost formations of the Emu Pool Supersuite within the Mt Edgar truncate the lithostratigraphy, indicating an intrusive relationship. Emu Pool Supersuite rocks have U-Pb zircon isotopic ages that range from 3321 Ma to 3299 Ma (Nelson, 2005).

Cleland Supersuite rocks have high potassium content and have a faint internal structure, the trace of which trends northwest approximately parallel the long axis of the mapped Cleland Supersuite exposure within the Mt Edgar dome. Macroscopic foliations strike approximately parallel to this long axis where visible (Collins, 1989). U-Pb zircon analyses within the Bishop Creek Monzogranite consistently yield isotopic ages of 3245-3233 Ma, often with a population of older ~3300 Ma zircons interpreted to be xenocrystic (e.g., Geochronology datasets 286 and 684 in Nelson, 2005).

Models for Mt Edgar Dome Development

The structures preserved in the greenstone belts that surround the Mt Edgar dome suggest a multiphase deformation history, although emphasis on different structures have led to differing genetic interpretations (Collins, 1989; Collins et al., 1998; Van Haaften and White, 1998; Collins and Van Kranendonk, 1999; Kloppenburg et al., 2001). One model for dome formation is partial convective overturn of the crust (Collins et al., 1998; Collins and Van Kranendonk, 1999; Sandiford et al., 2004; Van Kranendonk et al., 2004; François et al., 2014; Wiemer et al., 2018). Thermal weakening of a sialic lower crust cause dense supracrustal rocks to founder, leading to narrow greenstone keels that sink between broad granitic domes that rise passively. Collins

(1989) mapped localities within the greenstone belts to the west and southwest of the Mt Edgar dome as well as the dome interior, and observed two generations of structures that imply an early doming history. Isoclinal folding of the greenstone sequence is associated with the development of pervasive axial planar schistosity parallel to compositional layering (D1, F1, S1). Refolding of these isoclinal folds is associated with a variably developed axial planar crenulation cleavage (D2, F2, S2). The curved map pattern of supracrustal rocks to the west of the Mt Edgar dome (Fig. 1 A) is a structural dome thought to be responsible for D1 and D2 structures (Collins, 1989). The minimum age of this early dome structure is constrained by nearly undeformed 3.31 Ga plutons that crosscut it on the northern margin of the Mt Edgar granitic rocks. Further, Collins et al. (1998) mapped a triple junction between domes at the western edge of the Warrawoona Greenstone Belt and found a zone of vertical L-tectonites, which they interpreted to be a zone of greenstone foundering. Early structures are crosscut by a ringing shear zone that separates granitic dome rocks from the supracrustal rocks along the western, southern, and eastern margins of the Mt Edgar dome (D4 shear zone of Collins, 1989). Collins (1989) interpreted this shear zone to be the final exhumation event associated with dome formation, and observed that lineations locally plunge radially way from the dome margin.

Another model for dome formation is extensional core complex development followed by significant late-stage shortening and strike-slip deformation. In the East Pilbara Terrane, this mechanism was first proposed for the Shaw dome (Zegers, 1996; Zegers et al., 2001). In the Mt Edgar dome, Kloppenburg et al. (2001) found that lineations within the ringing shear zone uniformly trend southwest rather than plunging radially away from the dome margin. This nearly unidirectional lineation was interpreted as the extension direction along a detachment. In the Warrawoona greenstone belt to the southwest of the dome, Kloppenburg et al. (2001) mapped brittle-ductile thrusts that crosscut D1, D2, and D4 structures mapped by Collins (1989) and also observed pervasive dextral shearing within the central spine of the Warrawoona Greenstone Belt. These late structures were interpreted to represent the steepening of core complex dome walls and shuffling of dome blocks into their current configuration.

Field Data

Field observations and foliation measurements were collected at 267 locations within the Mt Edgar dome (Figs. 2 and 3). Outcrops are mostly large, low pavements or protruding ridges up to 4 m high. Foliations vary in their degree of development from too weak to discern to compositionally banded. Lineations are either too weak to evaluate or difficult to measure due to the pavement outcrop geometry.

Rocks of the Cleland Supersuite (Fig. 2 A) vary from homogeneous and nearly isotropic to compositionally banded with a strong foliation. Foliation is commonly defined by aligned plagioclase laths and biotite as well as stretched quartz blebs. Rare zones of leucosomes and melanosomes are observed. Rafts of high grade migmatitic gneisses are common, as are tabular, fine-grained granitic dikes or pegmatites that crosscut and distort foliation in the host rock. Foliations dip steeply and consistently strike northwest, nearly parallel to the long axis of the Bishop Creek Monzogranite (Fig. 3).

Rocks of the Emu Pool Supersuite (Fig. 2 B) are predominantly deformed granodiorites. An exception are the northernmost rocks of the dome, which are undeformed and have a very weak foliation defined by alignment of plagioclase. In the southern and southwest regions, the foliation is strongly developed and is defined by aligned mafic minerals and stretched quartz (Fig. 2 B-1).

Foliations dip steeply and exhibit highly variable strikes (Fig. 3). There is a slight preferred alignment towards the same northeast-southwest strike observed in the Cleland supersuite. The variability in strike is primarily caused by margin-parallel foliations close to the dome margin. Foliation also deviates from the dominant northwest strike in the Joorina Granodiorite (Fig. 3), in which many foliations strike northeast.

Rocks of the Tambina Supersuite (Fig. 2 C) have a gneissic foliation. They vary between banded migmatitic gneisses and more homogeneous tonalitic gneisses. In some localities within the banded gneisses, leucosomes are tightly folded and the gneissic foliation is axial planar to these folds (Fig. 2 C-1). Foliations in the southwest lobe strike northwest and dip steeply (Fig. 3). Foliations in the western lobe strike consistently northeast, but dip moderately to steeply to the northwest or southeast. At the very northern extent of the western lobe, vertical foliations strike northwest, parallel to foliations in the neighboring Cleland Supersuite.

Microstructures

Quartz and feldspar microstructures were observed at 83 localities within the Mt Edgar dome (Figs. 4-6). Samples selected for microstructural analysis are a representative subset of AMS stations (see Fig. 7 for locations). In outcrop, samples were collected from homogeneous host rock. Late-stage pegmatites, pockets of leucosome and melanosome, mafic xenoliths, and rafts of older granitic rocks were avoided. For a subset of samples, thin sections were prepared in the standard XZ fabric orientation. Due to sampling limitations, some thin sections were cut from 1-inch core rounds used in the AMS analysis. The orientation of magnetic foliation with respect to the thin section plane is documented in all photomicrographs (Figs. 4-6).

Microstructural Classification

Microstructural observations are used to interpret relative temperature conditions across the Mt Edgar dome. See Figures 4–6 for example interpretations. Aligned euhedral feldspar laths surrounded by large anhedral quartz grains with little internal distortion indicate magmatic flow (M) (e.g., Paterson et al., 1989; Rosenberg, 2001). Rare subgrain development in quartz has chessboard extinction morphology, indicating high quartz conditions (Kruhl, 1996). Submagmatic flow, in which solid-state deformation occurs in the presence of melt, is characterized by the dynamic recrystallization of quartz and/or feldspar. The divisions of Zibra et al. (2012) are adopted ("Type II" and "Type III" microstructures). Type II submagmatic microstructures (SM2) are characterized by the recrystallization of quartz into a mosaic of irregular, amoeboidal grains of varying apparent size, indicating the grain boundary migration recrystallization mechanism (Stipp et al., 2002). Quartz domains are aligned with foliation. Relict quartz grains display chessboard extinction, and the neighboring new grains often adopt the square structure of the chessboard extinction, indicating recrystallization at high temperature. Type III submagmatic microstructures (SM3) are characterized by the recrystallization of both quartz and feldspar. Quartz microstructures are similar to those of SM2 microstructures. Feldspar laths have curved boundaries. New recrystallized feldspar at lath margins is similar in size to subgrains, indicating the high temperature subgrain rotation recrystallization mechanism in feldspar (Rosenberg and Stünitz, 2003). In both SM2 and SM3 microstructures, fractures in single feldspar laths are infilled with quartz and feldspar, which suggests the presence of melt during deformation (Bouchez et al., 1992). Thin films of alkali feldspar are also observed, suggestive of the presence of melt (Sawyer, 1999). High-temperature solid state microstructures

(HT) are characterized by quartz ribbons separating partially recrystallized feldspar domains. Quartz grains have amoebodial boundaries, but with a smaller average recrystallized grain size than in submagmatic microstructures.

Cleland Supersuite Microstructures

Rocks of the Cleland Supersuite display a diversity of microstructures (Fig. 4). In the eastern region, plagioclase laths vary from ~1 mm to ~5 mm and are euhedral to subhedral. Samples with small plagioclase laths (~1 mm length) appear randomly oriented in a matrix of large poikilitic Alkali feldspar and elongate quartz grains (Fig. 4 A). In rocks with larger plagioclase laths, plagioclase is preferentially oriented parallel to lineation (Fig. 4 B). Alkali feldspar grains have deformation twins at the plagioclase-alkali feldspar boundaries, and myrmekite is common, suggesting a low-strain, high-temperature solid state overprint. Occasional quartz-filled fractures are observed in feldspars (Fig. 4 B). Quartz grains are elongate parallel to magnetic lineation and are internally deformed, often displaying a chessboard extinction pattern (Fig. 4 E). Quartz is locally recrystallized, and recrystallized grains are approximately the size of subgrains. New grains can be observed to be roughly square, with boundaries parallel to chessboard extinction boundaries in neighboring relict grains (Fig. 4 F). Elsewhere, grain boundaries are amoeboidal. In the central-west region of the Cleland Supersuite, recrystallized alkali feldspars with tartan twinning surround feldspar phenocrysts (Fig. 4 C). Phenocrysts are sometimes fractured and infilled with quartz and other minerals (Fig. 4 G) and myrmekite is common at feldspar grain boundaries (Fig. 4 H). Quartz is organized into recrystallized ribbons between feldspar domains. Quartz grain boundaries are highly irregular and amoeboidal, with some deformed relict grains remaining. In the southern region of the Cleland Supersuite, plagioclase, alkali feldspar, and quartz are all recrystallized and mixed to form a homogeneous polyphase aggregate (Fig 4 D). Grains are elongated in the direction of lineation.

Emu Pool Supersuite Microstructures

Rocks belonging to the Emu Pool Supersuite (Fig. 5) record a range of microstructures that overlaps with those of the Cleland Supersuite. In the northernmost exposure of the formation (Fig. 5 A), clots of interlocking plagioclase and alkali feldspar are separated by large quartz domains. Quartz grains are large (5-10 mm diameter) and record a chessboard extinction internal structure. Near the contact with Cleland rocks in the dome center, feldspars are aligned parallel to lineation (Fig. 5 B). Feldspars are occasionally fractured and infilled with quartz and other minerals, and are often lined with a thin film of late feldspar growth. Feldspars are locally, but rarely, recrystallized at lath boundaries. Interstitial quartz grains have chessboard extinction and are locally recrystallized (Fig. 5 B). Finely serrated grain boundaries are common, but no substantial fine-grained recrystallization has occurred at these boundaries. Feldspar is locally recrystallized along phenocryst margins. Quartz is organized into well-defined recrystallized ribbons subparallel to foliation. Quartz grain boundaries are amoeboidal and similarly sized to sub grains within larger relict grains. Within the Joorina Granodiorite Formation, plagioclase, alkali feldspar, and quartz are all recrystallized as a polyphase aggregate (Fig. 5 D). Many large grains of all three phases are interpreted as relict grains. Quartz grain boundaries are irregular and amoeboidal. Elsewhere in the Joorina granodiorite, the microstructure contains quartz ribbons wrapping around feldspar porphyroclasts similar to Figure 5 C.

Tambina Supersuite Microstructures

Rocks within the Tambina Supersuite (Fig. 6) record a narrower variety of microstructures than those from younger supersuites. Along the southwest margin of the Mt Edgar dome, some samples preserve rounded, aligned plagioclase phenocrysts surrounded by fully recrystallized quartz (Fig 6 A and B). Feldspars are partially recrystallized at their margins, and quartz-filled fractures in relict plagioclase phenocrysts are common. Quartz grain boundaries are amoeboidal. Elsewhere along the southwest margin, feldspars and quartz are both recrystallized into an aggregate (Fig. 6 C) with varying degrees of recrystallization. Along the southeast margin, plagioclase and alkali feldspar with tartan twinning are fully recrystallized along with quartz (Fig. 6 D). Relict quartz grains have faint chessboard extinction.

Microstructural Classification Results

Using the classification scheme described above, microstructures within all supersuites of the Mt Edgar dome indicate high-temperature, and in many cases melt-present, deformation conditions (Fig. 7). Submagmatic microstructures (SM2 and SM3) are the most commonly observed and occur throughout the dome, with especially high concentration in the Emu Pool formations. High temperature solid state fabrics (HT) occur along the southwest margin and within the center of the dome, both within the Joorina Granodiorite and the Bishop Creek Monzogranite. The eastern and northern regions of the dome preserve examples of magmatic fabric.

Anisotropy of Magnetic Susceptibility (AMS)

AMS Methodology

The anisotropy of magnetic susceptibility (AMS) is used to quantitatively map the orientation of foliation and lineation as well as fabric geometry (i.e., the relative strength of lineation and foliation within a sample). This study includes a total of 1,150 core specimens spread across 137 stations throughout the Mt Edgar dome. AMS is a proven tool for studying magmatic and solid-state foliation and lineation in granitic rocks (e.g., Borradaile, 1988; Cogné and Perroud, 1988; Bouchez et al., 1990; Vigneresse and Bouchez, 1997; Benn et al., 1998; Borradaile and Gauthier, 2003; Titus et al., 2005; Čečys and Benn, 2007; Kruckenberg et al., 2010). It is sufficiently sensitive to provide robust three-dimensional data for rocks with weak visible anisotropy, which makes it a useful petrophysical technique in situations – such as the Mt Edgar dome – where mesoscopic lineation is difficult to identify in the field due to rounded outcrop geometry and the overall weakness of fabric.

AMS data were collected on an AGICO KLYs-Kappabridge spinning low field magnetometer at the University of Wisconsin - Madison using AGICO Anisoft 4.2. Core specimens (24 mm diameter, 21 mm long) were drilled either in the field (AME16 prefix) or from oriented block samples (AME18 prefix). For field drilled sites, cores were sampled over at least a 2 meter area to account for outcrop heterogeneity. For a subset of block sampled sites, two block samples at least 3 meters apart were cored. AMS data for 4-14 core specimens was collected per station, and a mean ellipsoid at each station is used for analysis. The magnetic mineralogy in the Mt Edgar dome is dominantly titanomagnetite and maghemite for ferromagnetic (high susceptibility) specimens and biotite and chlorite for paramagnetic (low susceptibility) specimens (Roberts, 2020 and datasets accompanying this article).

An AMS datum is an ellipsoid that represents the directional anisotropy of susceptibility of a small core specimen. Susceptibility anisotropy is largely controlled by the preferred alignment of paramagnetic and/or ferromagnetic minerals, which often are aligned sub-parallel to the macroscopic foliation and lineation (Borradaile, 1988; Hrouda et al., 1997). The long and short axes of the AMS ellipsoid represent the magnetic lineation and pole to the magnetic foliation, respectively. Note that AMS does not necessarily record total finite strain, but does provide strain geometry information.

Two important parameters quantify the anisotropy and shape of the AMS ellipsoid. The anisotropy parameter P_j (Jelínek, 1981) describes the deviation from a sphere:

$$P_j = e^{\sqrt{2((lna_1 - lna_m)^2 + (lna_2 - lna_m)^2 + (lna_3 - lna_m)^2)}}$$

where a_1, a_2, and a_3 represent the long, intermediate, and short axis magnitudes, respectively, for the AMS ellipsoid. The quantity a_m is the geometric mean of a_1, a_2, and a_3. A sphere has a $P_j = 1$, and any non-spherical ellipsoid has $P_j > 1$.

The shape parameter T (Jelínek, 1981) describes the shape of the ellipsoid, from end-member oblate ($a_1 = a_2 > a_3$) to end-member prolate ($a_1 > a_2 = a_3$):

$$T = \frac{2(lna_1) - lna_2 - lna_3}{lna_1 - lna_3}, a_1 \neq a_3$$

T values between 0 and -1 are in the prolate field, or lineation-dominated (L>S). T values between 0 and 1 are in the oblate field, or foliation-dominated (S>L). T values close to 0 have an intermediate geometry (in strain terms, “plane strain”).

AMS Results: Orientation

The orientation of mean magnetic foliations and lineations for each station define a coherent, dome-wide structural pattern (Fig. 8). Orientations share similarities across all supersuites, with important second order variations, as shown in the small equal area nets at the top of Figure 8.

Cleland rocks have the most consistent orientation of foliation and lineation. Foliations are nearly all sub-vertical with a strike that is parallel to the long axis of the Bishop Creek Monzogranite. Lineations plunge moderately to subvertically and trend to the north-northwest. In map view, lineations plunge radially inward towards a central region of vertical lineations in the western region of the Bishop Creek Monzogranite (highlighted in Fig. 8 B).

Emu Pool rocks record a similar magnetic foliation and lineation to that of Cleland rocks, but with greater scatter. Two structural features are responsible for this variation. First, Emu Pool foliations within 2-3 km of the dome margin tend towards parallelism with the marginal contact. Margin-adjacent foliations therefore have variable strike and steep dips. Second, AMS lineations within the Joorina granodiorite define an arch structure that extends from near the dome center to the southwest margin (annotated in Fig. 8 B). At the Cleland-Joorina contact, lineations plunge moderately to the north towards the region of vertical lineations in the Cleland unit, and foliations strike northwest-southeast, parallel to adjacent Cleland rocks. Further to the southwest within the Joorina granodiorite, foliations dip shallowly to the northeast and lineations plunge shallowly to the north-northeast. Near the southwest margin – within Emu Pool Supersuite rocks between the two Tambina lobes – foliations strike northeast or east and dip steeply. Lineations plunge shallowly to the southwest.

The two lobes of the Tambina Supersuite have distinct structural patterns from one another that are consistent with compositional boundaries observed in the potassium content map (Fig 1 B) and large scale fold structures mapped by Collins (1989). The southwest lobe has orientations that closely resemble Cleland orientations. In map view, foliations dip steeply outward at the dome margin, whereas they dip steeply inward on the northeast half of the lobe. Foliations in neighboring Emu Pool rocks also dip inward towards the dome center, consistent with the large-scale fold outlined in the potassium content map.

The western lobe of the Tambina supersuite has foliations that generally strike parallel to the nearest contact with younger supersuites. On the eastern edge of the lobe, foliations strike northeast and dip moderately. Lineations plunge shallowly sub-parallel to foliation strike. At the northern edge of the lobe, subvertical foliations strike northwest, and lineations are subvertical, parallel with the adjacent Cleland AMS foliations and lineations. The relationship between these two fabric orientations within the western Tambina lobe is largely obscured by the 2.83 Ga Moolyella Adamellite of the Split Rock Supersuite. However, a transect of closely spaced stations (annotated in Fig. 8 A) on the western part of the lobe record a gradational change between the two fabric orientations within the western lobe. From south to north, foliation strike changes from northeast to northwest; dip changes from moderate to steep; lineation changes from shallowly southwest plunging to sub-vertical.

AMS Results: Ellipsoid Parameters

Results for the three invariant parameters of the AMS ellipsoid – bulk susceptibility Km, shape parameter T, and anisotropy parameter P_j – are summarized in Figure 9. The shape parameter T

spans the entire range from oblate (T = 1) to prolate (T = -1) (Fig. 9 B and C). There is a clear correlation between T and bulk susceptibility. High susceptibility stations exhibit an approximately even distribution in T that spans nearly the entire scale between oblate and prolate (Fig. 9 B). In contrast, low susceptibility measurements tend toward oblateness. In map view (Fig. 9 G), AMS stations near the southern, western, and eastern margins tend towards oblate shape, whereas the central and northern stations tend towards prolate shape.

The anisotropy parameter P_j ranges from 1.05 to 1.8, with most values less than 1.4. The mode P_j is 1.1. There is a correlation between P_j and susceptibility (Fig. 9 A); high susceptibility samples exhibit a greater range of P_j than low susceptibility samples. In map view, stations with high P_j are concentrated in the central Cleland Supersuite and Joorina Granodiorite Formation, along with a few scattered stations along the margins. Stations with low P_j are located along the margins with concentrations in the northern Emu Pool Supersuite formations as well as the Tambina Supersuite formations.

Discussion

Interpreting AMS results

The agreement between macroscopic field foliation (Fig. 3), the map patterns of compositional boundaries (Fig. 1 B), and magnetic foliation orientation determined from AMS (Fig. 8 A) suggests that AMS foliations and lineations can be generally interpreted as a reflection of macroscopic fabric orientation. The trace of fabric defined by elongate quartz grains and aligned feldspars in thin section is always consistent with the AMS lineation and foliation (see small equal area nets in Figs. 4–6), further confirming that macroscopic foliation is parallel to magnetic foliation.

It is critical to understand any bias of T or P due to magnetic mineralogy before interpreting T as strain geometry or P_j as strain magnitude (Borradaile, 1988). Magnetic mineralogy, which is reflected in bulk susceptibility Km, has been shown to sometimes bias T and/or P_j; for example, paramagnetic minerals such as biotite have a highly anisotropic crystalline structures that can bias the ellipsoid shape T toward oblate in some situations but not others (Kruckenberg et al., 2010).

A spatial comparison of T and mean susceptibility (Fig. 9 G and I) shows that the dependency of T on Km results from real differences in strain geometry across the dome rather than mineralogical bias. The southern half of the Mt Edgar dome is dominated by flattening AMS fabrics in both low and high susceptibility samples. The spatial consistency and systematic distribution of T within the Mt Edgar dome, regardless of mean susceptibility Km, suggests that magnetic mineralogy does not cause a strong bias in T. Instead, the correlation between Km and T results from the fact that lower susceptibility samples occur mostly within the flattening region of the dome. Given this analysis, variation in T is interpreted to indicate variation in the relative dominance of foliation and lineation (i.e., S, SL, L tectonites) among different stations. T is considered to be an approximate reflection of the geometry of finite strain for the last major deformation to occur within the dome.

A spatial analysis suggests that the dependency of P_j on Km (Fig. 9 A) reflects a mineralogical bias. In map view, this bias can be seen when comparing adjacent stations of different Km within the southwest lobe of the Tambina Supersuite. Higher susceptibility samples show a higher P_j for rocks that presumably experienced similar deformation. However, comparing P_j within domains of similar susceptibility may contain meaningful information. For example, the zone of high anisotropy within the Cleland Supersuite coincides with the zone of subvertical lineations (Fig. 8 B) and prolate geometry (Fig. 9 G). In this type of local comparison, P_j may relate to relative strain magnitude, but it is difficult to assess the reliability of this measure. At the dome scale, P_j is clearly not a reliable representation of total finite strain magnitude across the dome; strongly foliated rocks on the dome margin tend to have lower P_j values than weakly foliated rocks in the dome center.

In summary, the AMS dataset provides robust information about the orientation and geometry of strain, but not strain magnitude. AMS orientations and ellipsoid geometry are interpreted to represent the final major deformation experienced by any given specimen, since AMS data can be reset or overprinted over the course of continuing strain (Benn, 1994).

Internal structure of the Mt Edgar dome

Magnetic fabric data derived from AMS reveal a coherent dome-wide structural pattern (Fig. 10). The Cleland supersuite, much of the Emu Pool supersuite, and the southwest lobe of the Tambina supersuite have a dominant northwest striking, steeply dipping foliation and sub-vertical lineation. This preferred orientation is most pronounced in the Cleland supersuite; magnetic lineations point radially inward toward a central zone of vertical magnetic lineations and prolate AMS ellipsoids (L>>S). Two large-scale structures on the western and southwestern parts of the dome deviate from this dome-wide preferred orientation: 1) An arch structure in the Emu Pool-aged Joorina Granodiorite extends from the southern contact of Cleland units to the southwest margin (the "Joorina arch"); and 2) Large scale fold structures are present in both lobes of the Tambina supersuite.

The Joorina arch is characterized by prolate to plane strain AMS ellipsoids, with magnetic lineations that plunge shallowly inward near the center of the dome and shallowly outward near the dome margin. Foliations dip shallowly to the north-northeast near the dome center, but are parallel to the Tambina contact near the dome margin. The Joorina arch is in structural continuity with the surrounding Cleland and Emu Pool units; foliations and lineations transition gradually into the dominant dome-wide preferred orientation. The Joorina arch structure is interpreted to be a zone of lateral flow emanating from the dome center to the dome margin, diving Tambina Supersuite rocks into two lobes.

The foliations in both lobes of the Tambina Supersuite are consistent with large-scale folding of a pre-existing fabric, as observed by Collins (1989). The southwest lobe is a single isoclinal fold. Foliations dip inward towards the dome center on the northeast limb of the fold and outward on the southwest limb of the fold. This fold pattern continues into adjacent Emu Pool rocks to the northeast. The large-scale structure in the western lobe is a series of upright folds. In the eastern part of the lobe, foliations striking northeast are axial planar to the large-scale folds, and subhorizontal lineations are interpreted to represent hinge-parallel extension.

The northwest part of the lobe has a significantly different foliation that strikes northwest and dips subvertically. The intersection of this foliation and the foliation in the rest of the lobe is partially obscured by the 2.83 Ga Moolyella Adamellite, but a transect of AMS stations in the western part of the lobe show a gradational change between them. This change in orientation has previously been interpreted as a strain gradient out of a hypothesized northeast-southwest striking shear zone (The "Beaton Well shear zone" of Kloppenburg et al., 2001). Given the parallelism of these AMS fabrics to adjacent Cleland Supersuite rocks, it is likely that they represent strain at the margin of the Tambina lobe during Cleland-age deformation.

The structures within the western lobe Tambina Supersuite are truncated to the south and west by foliations that are subparallel to the dome margin. Margin-parallel foliations exist along the western, southwestern, southeastern, and eastern margins of the dome, consistently deflecting the dome-wide fabric. These data are in agreement with Collins (1989), who interpreted this sheared margin to be the last phase of dome deformation (D4).

Assessing the possibility of a Neoarchean overprint

The presence of a strong preferred orientation of foliation within the Mt Edgar dome raises the question: Do foliations and lineations represent a northeast-southwest shortening overprint that is unrelated to dome formation? Previous structural studies have noted the presence of thrust faults in the surrounding greenstone belts that record northeast-southwest shortening (Van Haaften and White, 1998).

Several aspects of our data indicate that the field foliations and AMS ellipsoids predominantly reflect the structures associated with Mt Edgar dome formation. First, the northwest striking foliation is best developed in the Cleland Supersuite, and is more scattered or non-existent in other parts of the dome (Figs. 3 and 8). This variation is not consistent with a regional, penetrative foliation overprint. Second, the Cleland unit is itself elongate parallel to the strike of foliation, and lineations plunge radially inward toward a central location. These two observations suggest that the preferred alignment within the Cleland unit resulted primarily from internal flow – and associated syn-doming strain – rather than a planar, externally imposed deformation.

Third, foliations and lineations are parallel to Tambina boundaries in the southwest and western regions of the dome. The fact that foliations and lineations deviate from the dome-wide orientation at these contacts is not consistent with a late-stage overprint. Finally, the dominant northwest striking foliation is deflected by strong margin-parallel foliation along the domes southeastern, southwestern, and western boundaries (The D4 of Collins, 1989). This deflection can be most clearly seen in the southeastern region of the dome in the AMS dataset (Fig. 8 A). The dome-wide fabrics predate or are contemporaneous with the marginal foliations. This cross-cutting relationship has been corroborated in the field (Collins et al., 1998).

Melt-assisted flow of dome rocks

Microstructural observations suggest that rocks of all supersuite ages deformed at high temperature, near-solidus conditions. In many samples, microfabrics are characteristic of melt-present deformation. Deformation experiments of partially molten rock suggest that small (<0.07) melt fractions can drastically lower rock strength (Rosenberg and Handy, 2005). Evidence of wide-spread melt-present deformation in the Mt Edgar dome therefore implies that dome rocks were significantly thermally weakened and would have flowed readily. The thermal weakening of sialic crust has been a central aspect of the convective overturn model, and partial melting of rocks during dome exhumation is typically included in conceptual models (Collins et al., 1998; Sandiford et al., 2004; Van Kranendonk et al., 2004). In numerical experiments of dome formation by convective overturn, partial melting plays a key role in mobilizing the lower crust (François et al., 2014). The microstructural data presented here are consistent with these models.

Timing of Dome Flow

Although microstructural analysis suggests evidence for melt-assisted and high-temperature flow across the Mt Edgar dome, several critical questions concerning timing remains: 1) When did melt-assisted flow happen? and 2) Did melt-assisted flow happen all at once or in stages? Several lines of evidence point towards synchronous, dome-wide flow during Cleland magmatism.

First, the dome-wide structural pattern is at least suggestive of a deformation event that affected all but the most northern units of the dome. The dominant northwest-striking foliation exists in rocks of all ages and is most tightly clustered in the Cleland Supersuite, suggesting that deformation/emplacement of the Cleland supersuite is central to the dome-wide structure. Structures are continuous across unit boundaries with the exception of the D4 shear zone at the dome margin. Radial lineations within the Cleland Supersuite become shallower towards the south, and continue into the Joorina arch. This structural continuity implies that the Cleland and Emu Pool supersuites deformed at the same time.

Second, rocks of Emu Pool Supersuite and Tambina Supersuite age are interfolded in the western lobe of the Tambina Supersuite and the isoclinal fold structure within the southwest lobe of the Tambina Supersuite continues into Emu Pool rocks to the northeast. Systematic variations in shape parameter T ignore the Tambina-Emu Pool contact on the southwest margin, indicating that significant deformation occurred after emplacement of both. These structures must have formed during or after Emu Pool magmatism.

Third, microstructural evidence from the D4 shear zone suggests similar high-temperature conditions to the rest of the dome. The D4 shear zone deflects or crosscuts earlier structures, and should represent the lowest temperature part of the system since it was structurally above the dome rocks and in contact with colder greenstones. The observation that the D4 shearing occurred under near-solidus conditions implies that the entire dome was at near-solidus conditions during this final phase of dome-related deformation.

Evidence for significant dome-wide dome flow during Cleland Supersuite magmatism contrasts with previous work, which suggested most deformation occurred during Emu Pool magmatism. Previous mapping efforts found that the D4 shear zone crosscut 3.31 Ga plutons on the southwest margin and was crosscut by the 3.31 Ga Wilina pluton on the southeast margin (Williams and Collins, 1990; Collins et al., 1998), thereby bracketing deformation to Emu Pool Supersuite age. However, subsequent mapping (Hickman, 2016) shows that the Wilina Pluton intruded greenstone rocks just outside the D4 shear zone.

François et al. (2014) investigated the timing of dome formation through U-Pb zircon and monazite geochronology paired with metamorphic petrology and thermomechanical models. Metamorphic zircon within two granulite samples from a metasedimentary raft in Emu Pool rocks near the core of the Mt Edgar dome yield U-Pb isotopic ages of 3311.9 ± 4.9 Ma and 3314.6 ± 3.3 Ma. They interpret these ages to represent the deepest part of a rapid (~5 m.y.) cycle of burial and exhumation at ca. 3315–3310 Ma. Their thermomechanical models suggest that this rapid exhumation is possible. However, rims on some zircons yielded younger discordant isotopic ages, including one at 3264 ± 2 Ma, suggesting a possible later event of Cleland Supersuite age.

Proposed structural development of the Mt Edgar dome

In the context of previous structural work and published U-Pb zircon ages, a model for the structural development of the Mt Edgar dome is proposed (Fig. 11):

- Tambina Supersuite rocks were emplaced into the crust as either a single body or a series of magmatically related intrusions at 3.47-3.41 Ga.

- Emu Pool at 3.32–3.29 Ga magmatism was voluminous, sufficient for a buoyancy-driven dome to form in the deep crust. Tambina rocks were reheated and migmatized at this time, in part due to decompression at the roof of domes. Migmatization likely localized deformation along the margins of the Mt Edgar dome that have Tambina rocks, controlling subsequent dome asymmetry. The D4 shear zone of Collins (1989) initiated during this strain localization.

- Late Emu Pool and Cleland magmas intruded the core of the dome from 3.29 - 3.23 Ga, reheating and remobilizing earlier units. Dome-wide melt-assisted flow resulted towards the end of this magmatism, characterized by vertical ascent into the upper crust and lateral flow to the southwest near the roof of the dome. The duration of this flow remains unconstrained, but it continued as Cleland Supersuite rocks fully crystallized, as indicated by the presence of high temperature solid-state fabrics. During the emplacement of these younger formations, Tambina Supersuite gneisses and Emu Pool Supersuite tonalites were interfolded and flattened against the margin and flowed out of the way. The Joorina arch is interpreted to be a record of this lateral flow from the dome center to the dome margins. Internal flow within the dome caused further dome amplification and continued deformation along the D4 shear zone of (Collins, 1989).

The data presented in this paper indicate that the Mt Edgar dome rose as an asymmetric diapiric structure through the supracrustal sequence. L>S tectonites with subvertical lineations in the core of the dome, S>L tectonites with margin foliation parallel foliations along the sheared margin, and zones lateral flow between the core and margin are all predictions of a diapiric model (Mareschal and West, 1980). The dome-wide structure and microstructural data are broadly consistent with the convective overturn model of Collins et al. (1998) and the numerical models of François et al. (2014), although the timing of the final dome-forming event appears to be 50 m.y. later than previously proposed. The discrepancy in timing of deformation between this study and previous studies should motivate further geochronological and petrological study.

Conclusion

The Mt Edgar dome has a coherent internal structure that resembles an asymmetric diapiric dome with significant internal, melt-assisted flow. Anisotropy of magnetic susceptibility (AMS) data document for the first time the orientation of lineation and the fabric geometry (S>L, SL, L>S) within the dome. Lineations within the dome core plunge radially inward towards a zone of vertical L-tectonites. In the southwest dome region, lineations plunge shallowly to define an arch that extends from the dome center to the southwest margin. Marginal fabrics are dominated by S>L tectonites. The oldest units in the dome are folded against the dome margin. Microstructural observations suggest that all dome rocks deformed under high temperature, near solidus temperatures.

Structural relationships and existing geochronology data suggest that melt-assisted dome flow occurred synchronously across the dome during Cleland Supersuite magmatism. This deformation was the last of several dome-forming events that have long been recognized in the East Pilbara Terrane. The data presented in this paper provide empirical evidence that the East

Pilbara domes formed under a regime of thermal weakening and bulk upwards rise of granitic material. Models that invoke this process suggest that this thermal weakening would lead to rapid crustal overturn (Sandiford et al., 2004; François et al., 2014), although the duration of doming remains poorly constrained.

Acknowledgements

This work was funded by NSF EAR 2020057 and the Wisconsin Alumni Research Foundation (WARF). Thank you to the Structural Geology and Tectonics group at UW-Madison and A. Bauer, H. Sone, J. Davis, L. Goodwin, and V. Chatzaras for providing helpful feedback. B. Hess and D. Rogers prepared thin sections. K. Korman, E. Lahr, R. Salerno, C. Idzikowski, and R. Key assisted in the field. Thank you to the Brooks family for all your logistical help, advice, and good company. Thanks also to Yarrie and Corunna Downs stations for land access. All original data mentioned in this publication, as well as a fully commented R project that reproduces many of the maps and figure elements in this paper can be viewed and downloaded at: https://osf.io/jcqgy/?view_only=4dc3d82192cf41f7b3119ca97b50112d.

Bibliography

Barley, M., Pickard, A., 1999. An extensive, crustally-derived, 3325 to 3310 Ma silicic volcanoplutonic suite in the eastern Pilbara Craton: evidence from the Kelly Belt, McPhee Dome and Corunna Downs Batholith. Precambrian Research 96, 41–62.

Bédard, J.H., 2003. Evidence for Regional-Scale, Pluton-Driven, High-Grade Metamorphism in the Archaean Minto Block, Northern Superior Province, Canada. The Journal of Geology 111, 183–205.

Bédard, J.H., 2006. A catalytic delamination-driven model for coupled genesis of Archaean crust and sub-continental lithospheric mantle. Geochimica et Cosmochimica Acta 70, 1188–1214.

Bédard, J.H., 2018. Stagnant lids and mantle overturns: Implications for Archaean tectonics, magmagenesis, crustal growth, mantle evolution, and the start of plate tectonics. Geoscience Frontiers 9, 19–49.

Benn, K., 1994. Overprinting of magnetic fabrics in granites by small strains: numerical modelling. Tectonophysics 233, 153–162.

Benn, K., Ham, N.M., Pignotta, G.S., Bleeker, W., 1998. Emplacement and deformation of granites during transpression: magnetic fabrics of the Archean Sparrow pluton, Slave Province, Canada. Journal of Structural Geology 20, 1247–1259.

Bickle, M.J., Bettenay, L.F., Chapman, H.J., Groves, D.I., McNaughton, N.J., Campbell, I.H., de Laeter, J.R., 1992. Origin of the 3500-3300 Ma calc-alkaline rocks in the Pilbara Archaean: isotopic and geochemical constraints from the Shaw Batholith. Precambrian Research 60, 117–149.

Blewett, R.S., 2002. Archaean tectonic processes: a case for horizontal shortening in the North Pilbara Granite-Greenstone Terrane, Western Australia. Precambrian Research 113, 87–120.

Borradaile, G., Gauthier, D., 2003. Emplacement of an Archean gneiss dome, northern Ontario, Canada: inflation inferred from magnetic fabrics. Tectonics 22.

Borradaile, G.J., 1988. Magnetic susceptibility, petrofabrics and strain. Tectonophysics 156, 1–20.

Bouchez, J.L., Delas, C., Gleizes, G.r., Nédélec, A., Cuney, M., 1992. Submagmatic microfractures in granites. Geology 20, 35-38.

Bouchez, J.L., Gleizes, G., Djouadi, T., Rochette, P., 1990. Microstructure and magnetic susceptibility applied to emplacement kinematics of granites: the example of the Foix pluton (French Pyrenees). Tectonophysics 184, 157–171.

Bouhallier, H., Chardon, D., Choukroune, P., 1995. Strain patterns in Archaean dome-and-basin structures: the Dharwar craton (Karnataka, South India). Earth and Planetary Science Letters 135, 57–75.

Čečys, A., Benn, K., 2007. Emplacement and deformation of the ca. 1.45 Ga Karlshamn granitoid pluton, southeastern Sweden, during ENE-WSW Danopolonian shortening. International Journal of Earth Sciences 96, 397–414.

Chardon, D., Choukroune, P., Jayananda, M., 1998. Sinking of the Dharwar Basin (South India): implications for Archaean tectonics. Precambrian Research 91, 15-39.

Cogné, J.-P., Perroud, H., 1988. Anisotropy of magnetic susceptibility as a strain gauge in the Flamanville granite, NW France. Physics of the Earth and Planetary Interiors 51, 264–270.

Collins, W.J., 1989. Polydiapirism of the Archean Mount Edgar Batholith, Pilbara Block, Western Australia. Precambrian Research 43, 41–62.

Collins, W.J., 1993. Melting of Archaean sialic crust under high aH2O conditions: genesis of 3300 Ma Na-rich granitoids in the Mount Edgar Batholith, Pilbara Block, Western Australia. Precambrian Research 60, 151–174.

Collins, W.J., Van Kranendonk, M.J., 1999. Model for the development of kyanite during partial convective overturn of Archean granite-greenstone terranes: The Pilbara Craton, Australia. Journal of Metamorphic Geology 17, 145–156.

Collins, W.J., Van Kranendonk, M.J., Teyssier, C., 1998. Partial convective overturn of Archaean crust in the east Pilbara Craton, Western Australia: driving mechanisms and tectonic implications. Journal of Structural Geology 20, 1405–1424.

Doublier, M., Johnson, S., Gessner, K., Howard, H., Chopping, R., Smithies, R.H., Martin, D., Kelsey, D., Haines, P., Hickman, A., Czarnota, K., Southby, C., Champion, D., Huston, D., Calvert, A., Kohanpour, F., Moro, P., Costelloe, R., Fomin, T., Sykes, J., 2020. Basement architecture from the Pilbara Craton to the Aileron Province: new insights from deep seismic reflection line 18GA-KB1.

François, C., Philippot, P., Rey, P., Rubatto, D., 2014. Burial and exhumation during Archean sagduction in the East Pilbara Granite-Greenstone Terrane. Earth and Planetary Science Letters 396, 235–251.

Gardiner, N.J., Hickman, A.H., Kirkland, C.L., Lu, Y., Johnson, T., Zhao, J.-X., 2017. Processes of Crust Formation in the Early Earth Imaged through Hf isotopes from the East Pilbara Terrane. Precambrian Research.

Green, M.G., Sylvester, P.J., Buick, R., 2000. Growth and recycling of early Archaean continental crust: geochemical evidence from the Coonterunah and Warrawoona Groups, Pilbara Craton, Australia. Tectonophysics 322, 69–88.

Harris, L.B., Godin, L., Yakymchuk, C., 2012. Regional shortening followed by channel flow induced collapse: A new mechanism for “dome and keel” geometries in Neoarchaean granite-greenstone terrains. Precambrian Research 212-213, 139-154.

Hickman, A.H., 1984. Archaean diapirism in the Pilbara Block, Western Australia, in: Kroner, A., Greiling, R. (Eds.), Precambrian Tectonics Illustrated, pp. 113–127.

Hickman, A.H., 2012. Review of the Pilbara Craton and Fortescue Basin, Western Australia: Crustal evolution providing environments for early life. Island Arc 21, 1–31.

Hickman, A.H., 2016. Interpreted bedgrock geology of the east Pilbara Craton. Geological Survey of Western Australia.

Hickman, A.H., Van Kranendonk, M.J., 2012. Early Earth evolution: evidence from the 3.5-1.8 Ga geological history of the Pilbara region of Western Australia. Episodes 35, 283–297.

Hrouda, F., Schulmann, K., Suppes, M., Ullemayer, K., De Wall, H., Weber, K., 1997. Quantitive relationship between low-field AMS and phyllosilicate fabric: a review. Physics and Chemistry of the Earth 22, 153–156.

Jelínek, V., 1981. Characterization of the magnetic fabric of rocks. Tectonophysics 79, T63–T67.

Johnson, T.E., Brown, M., Gardiner, N.J., Kirkland, C.L., Smithies, R.H., 2017. Earth's first stable continents did not form by subduction. Nature 543, 239–242.

Kisters, A.F.M., Anhaeusser, C.R., 1995. Emplacement features of Archaean TTG plutons along the southern margin of the Barberton greenstone belt, South Africa. Precambrian Research 75, 1-15.

Kloppenburg, A., White, S.H., Zegers, T.E., 2001. Structural evolution of the Warrawoona Greenstone Belt and adjoining granitoid complexes, Pilbara Craton, Australia: implications for Archaean tectonic processes. Precambrian Research 112, 107–147.

Kruckenberg, S.C., Ferré, E.C., Teyssier, C., Vanderhaeghe, O., Whitney, D.L., Seaton, N.C., Skord, J.A., 2010. Viscoplastic flow in migmatites deduced from fabric anisotropy: An example from the Naxos dome, Greece. Journal of Geophysical Research: Solid Earth 115.

Kruhl, J., 1996. Prism-and basal-plane parallel subgrain boundaries in quartz: A microstructural geothermobarometer. Journal of metamorphic Geology 14, 581–589.

Lana, C., Tohver, E., Cawood, P., 2010. Quantifying rates of dome-and-keel formation in the Barberton granitoid-greenstone belt, South Africa. Precambrian Research 177, 199–211.

Liu, T., Wei, C., 2018. Metamorphic evolution of Archean ultrahigh-temperature mafic granulites from the western margin of Qian’an gneiss dome, eastern Hebei Province, North China Craton: Insights into the Archean tectonic regime. Precambrian Research 318, 170-187.

Mareschal, J.-C., West, G.F., 1980. A model for Archean tectonism. Part 2. Numerical models of vertical tectonism in greenstone belts. Canadian Journal of Earth Sciences 17, 60–71.

Moore, W.B., Webb, A.A.G., 2013. Heat-pipe Earth. Nature 501, 501-505.

Nelson, D.R., 1999. Compilation of SHRIMP U-Pb zircon geochronology date, 1998: Western Australia Geological Survey.

Nelson, D.R., 2001. Compilation of SHRIMP U–Pb zircon geochronology data, 2000: Western Australia Geological Survey. Record.

Nelson, D.R., 2005. Compilation of geochronology data: Western Australia Geological Survey. June.

Nijman, W., Kloppenburg, A., de Vries, S.T., 2017. Archaean basin margin geology and crustal evolution: an East Pilbara traverse. Journal of the Geological Society 174, 1090–1112.

Nutman, A.P., Bennett, V.C., Friend, C.R.L., 2015. Proposal for a continent 'Itsaqia' amalgamated at 3.66 Ga and rifted apart from 3.53 Ga: Initiation of a Wilson Cycle near the start of the rock record. American Journal of Science 315, 509.

Paterson, S.R., Vernon, R.H., Tobisch, O.T., 1989. A review of criteria for the identification of magmatic and tectonic foliations in granitoids. Journal of structural geology 11, 349–363.

Pawley, M., Van Kranendonk, M., Collins, W., 2004. Interplay between deformation and magmatism during doming of the Archaean Shaw granitoid complex, Pilbara Craton, Western Australia. Precambrian Research 131, 213-230.

Piper, J., 2018. Dominant Lid Tectonics behaviour of continental lithosphere in Precambrian times: Palaeomagnetism confirms prolonged quasi-integrity and absence of supercontinent cycles. Geoscience Frontiers 9, 61–89.

Piper, J.D., 2013. A planetary perspective on Earth evolution: lid tectonics before plate tectonics. Tectonophysics 589, 44–56.

Polat, A., Kokfelt, T., Burke, K.C., Kusky, T.M., Bradley, D.C., Dziggel, A., Kolb, J., 2016. Lithological, structural, and geochemical characteristics of the Mesoarchean T{â}rtoq greenstone belt, southern West Greenland, and the Chugach–Prince William accretionary complex, southern Alaska: evidence for uniformitarian plate-tectonic processes. Canadian Journal of Earth Sciences 53, 1336–1371.

Polat, A., Wang, L., Appel, P.W.U., 2015. A review of structural patterns and melting processes in the Archean craton of West Greenland: Evidence for crustal growth at convergent plate margins as opposed to non-uniformitarian models. Tectonophysics 662, 67–94.

Ramsay, J.G., 1989. Emplacement kinematics of a granite diapir: the Chindamora batholith, Zimbabwe. Journal of Structural Geology 11, 191–209.

Roberts, N.M., 2020. Internal Fabrics and Marginal Deformation of the Paleoarchean Mt Edgar Dome, East Pilbara Terrane, Western Australia: Structural Constraints on Crustal Flow in the Early Earth. The University of Wisconsin-Madison.

Rosenberg, C., Handy, M., 2005. Experimental deformation of partially melted granite revisited: implications for the continental crust. Journal of metamorphic Geology 23, 19-28.

Rosenberg, C.L., 2001. Deformation of partially molten granite: a review and comparison of experimental and natural case studies. International Journal of Earth Sciences 90, 60-76.

Rosenberg, C.L., Stünitz, H., 2003. Deformation and recrystallization of plagioclase along a temperature gradient: an example from the Bergell tonalite. Journal of Structural Geology 25, 389-408.

Sandiford, M., Van Kranendonk, M.J., Bodorkos, S., 2004. Conductive incubation and the origin of dome-and-keel structure in Archean granite-greenstone terrains: A model based on the eastern Pilbara Craton, Western Australia. Tectonics 23.

Sawyer, E.W., 1999. Criteria for the recognition of partial melting. Physics and Chemistry of the Earth, Part A: Solid Earth and Geodesy 24, 269-279.

Smithies, R.H., Champion, D.C., Cassidy, K.F., 2003. Formation of Earth's early Archaean continental crust. Precambrian Research 127, 89–101.

Smithies, R.H., Champion, D.C., Van Kranendonk, M.J., Howard, H.M., Hickman, A.H., 2005. Modern-style subduction processes in the Mesoarchaean: geochemical evidence from the 3.12 Ga Whundo intra-oceanic arc. Earth and Planetary Science Letters 231, 221–237.

Smithies, R.H., Ivanic, T.J., Lowrey, J.R., Morris, P.A., Barnes, S.J., Wyche, S., Lu, Y.-J., 2018. Two distinct origins for Archean greenstone belts. Earth and Planetary Science Letters 487, 106–116.

Stipp, M., Stünitz, H., Heilbronner, R., Schmid, S.M., 2002. The eastern Tonale fault zone: a 'natural laboratory'for crystal plastic deformation of quartz over a temperature range from 250 to 700 C. Journal of Structural Geology 24, 1861–1884.

Thébaud, N., Rey, P.F., 2013. Archean gravity-driven tectonics on hot and flooded continents: Controls on long-lived mineralised hydrothermal systems away from continental margins. Precambrian Research 229, 93–104.

Titus, S.J., Clark, R., Tikoff, B., 2005. Geologic and geophysical investigation of two fine-grained granites, Sierra Nevada Batholith, California: Evidence for structural controls on emplacement and volcanism. Geological Society of America Bulletin 117, 1256.

Van Haaften, W.M., White, S.H., 1998. Evidence for multiphase deformation in the Archean basal Warrawoona Group in the Marble Bar area, east Pilbara, Western Australia. Precambrian Research 88, 53–66.

Van Kranendonk, M.J., 2006. Revised lithostratigraphy of Archean supracrustal and intrusive rocks in the northern Pilbara Craton, Western Australia. Geological Survey of Western Australia.

Van Kranendonk, M.J., 2010. Two types of Archean continental crust: Plume and plate tectonics on early earth. American Journal of Science 310, 1187–1209.

Van Kranendonk, M.J., 2011. Cool greenstone drips and the role of partial convective overturn in Barberton greenstone belt evolution. Journal of African Earth Sciences 60, 346–352.

Van Kranendonk, M.J., Collins, W.J., Hickman, A., Pawley, M.J., 2004. Critical tests of vertical vs. horizontal tectonic models for the Archaean East Pilbara Granite-Greenstone Terrane, Pilbara Craton, Western Australia. Precambrian Research 131, 173–211.

Van Kranendonk, M.J., Hugh Smithies, R., Hickman, A.H., Champion, D.C., 2007. Review: Secular tectonic evolution of Archean continental crust: interplay between horizontal and vertical processes in the formation of the Pilbara Craton, Australia. Terra Nova 19, 1–38.

Vigneresse, J.L., Bouchez, J.L., 1997. Successive Granitic Magma Batches During Pluton Emplacement: the Case of Cabeza de Araya (Spain). Journal of Petrology 38, 1767–1776.

Webb, A.A.G., Müller, T., Zuo, J., Haproff, P.J., Ramírez-Salazar, A., 2020. A non–plate tectonic model for the Eoarchean Isua supracrustal belt. Lithosphere 12, 166-179.

Whitney, D.L., Teyssier, C., Rey, P., Buck, W.R., 2013. Continental and oceanic core complexes. GSA Bulletin 125, 273-298.

Whitney, D.L., Teyssier, C., Vanderhaeghe, O., 2004. Gneiss domes and crustalflow. Gneiss domes in orogeny 380, 15.

Wiemer, D., Schrank, C.E., Murphy, D.T., Hickman, A.H., 2016. Lithostratigraphy and structure of the early Archaean Doolena Gap greenstone belt, East Pilbara Terrane, Western Australia. Precambrian Research 282, 121–138.

Wiemer, D., Schrank, C.E., Murphy, D.T., Wenham, L., Allen, C.M., 2018. Earth's oldest stable crust in the Pilbara Craton formed by cyclic gravitational overturns. Nature Geoscience 11, 357.

Williams, I.S., Collins, W.J., 1990. Granite-greenstone terranes in the Pilbara Block, Australia, as coeval volcano-plutonic complexes; Evidence from U-Pb zircon dating of the Mount Edgar Batholith. Earth and Planetary Science Letters 97, 41-53.

Yin, A., 2004. Gneiss domes and gneiss dome systems. Geological Society of America Special Papers 380, 1–14.

Zegers, T.E., 1996. Structural, kinematic and metallogenic evolution of selected domains of the Pilbara granitoid-greenstone terrain: implications for mid Archean tectonic regimes. Utrecht University.

Zegers, T.E., Nelson, D.R., Wijbrans, J.R., White, S.H., 2001. SHRIMP U-Pb zircon dating of Archean core complex formation and pancratonic strike-slip deformation in the East Pilbara Granite-Greenstone Terrain. Tectonics 20, 883–908.

Zegers, T.E., van Keken, P.E., 2001. Middle Archean continent formation by crustal delamination. Geology 29, 1083–1086.

Zegers, T.E., White, S.H., de Keijzer, M., Dirks, P.H., 1996. Extensional structures during deposition of the 3460 Ma Warrawoona Group in the eastern Pilbara Craton, Western Australia. Precambrian Research 80, 89–105.
Zegers, T.E., Wijbrans, J.R., White, S.H., 1999. 40Ar/39Ar age constraints on tectonothermal events in the Shaw area of the eastern Pilbara granite–greenstone terrain (W Australia): 700 Ma of Archean tectonic evolution. Tectonophysics 311, 45–81.
Zibra, I., Kruhl, J.H., Montanini, A., Tribuzio, R., 2012. Shearing of magma along a high-grade shear zone: Evolution of microstructures during the transition from magmatic to solid-state flow. Journal of Structural Geology 37, 150-160.
Zibra, I., Lu, Y., Clos, F., Weinberg, R., Peternell, M., Wingate, M., Prause, M., Schiller, M., Tilhac, R., 2020. Regional-scale polydiapirism predating the Neoarchean Yilgarn Orogeny. Tectonophysics 779, 228375.

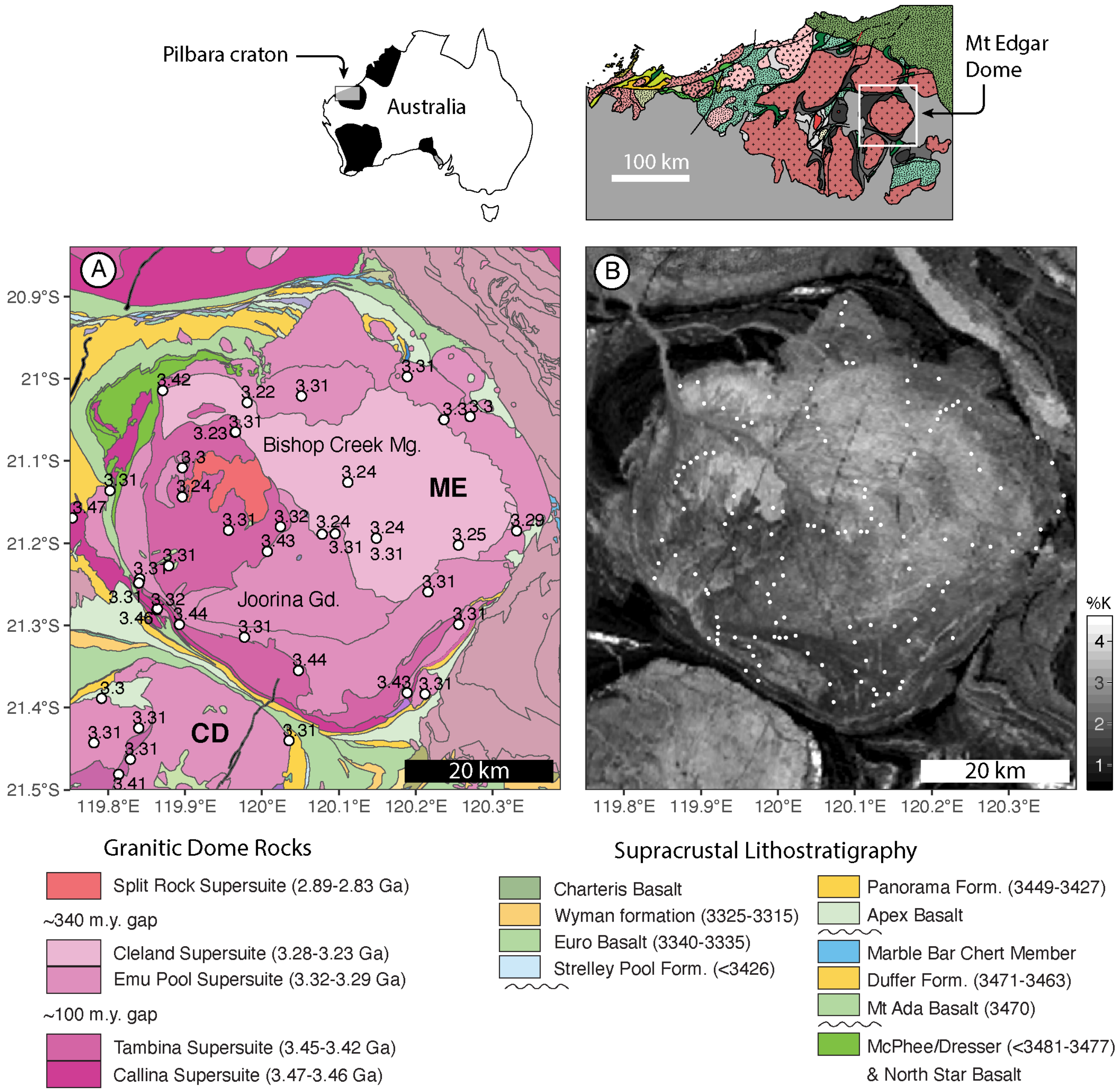

Figure 1. Geologic and Potassium content maps of the Mt Edgar dome. Top diagrams show location in Western Australia of the Mt Edgar dome (modified from Van Kranendonk et al., 2007). A) Interpreted bedrock geology of the Mt Edgar dome (ME) and northern Corunna Downs dome (CD) (modified from Hickman, 2016). A legend for the geologic map is at the bottom of the figure. Labeled white dots are U-Pb zircon SHRIMP ages (Nelson, 1999; 2001; 2005) in billions of years. Joorina Gd: Joorina Granodiorite, an Emu Pool Supersuite Formation. Bishop Creek Mg: Bishop Creek Monzogranite, a Cleland Supersuite Formation B) Potassium content map based on flyover Gamma Ray spectroscopy (Geological Survey of Western Australia). White dots are locations of AMS stations in this study.

Figure 2. Field photographs from the Mt Edgar dome. A) Cleland Supersuite rocks: A-1) Feldspar megacryst is aligned parallel to foliation. Smaller feldspar phenocryst laths define the foliation. A-2) Schleren banding is offset by pegmatites (outlined). A-3) Example of a raft of banded gneiss within weakly foliated granite. Contact is sharp (outlined), with some injection of granite into the raft parallel to the gneissic foliation. A-4) Macroscopic fabric defined by rounded aligned feldspars, biotite, and elongate quartz blebs. B) Emu Pool Supersuite rocks: B-1) Gneissic foliation in the Joorina Granodiorite defined by quartz ribbons, elongate feldspar domains, and smeared biotite. B-2) Foliation defined by aligned euhedral amphibole and feldspars. C) Tambina Supersuite rocks: C-1) Migmatitic gneiss. Leuscosomes are tightly folded (outlined in white), and gneissic foliation is axial planar to fold. C-2) Gneissic fabric typical of non-migmatized localities, showing incipient mineral banding. C-3) Swirly banded migmatitic gneiss in a pavement outcrop.

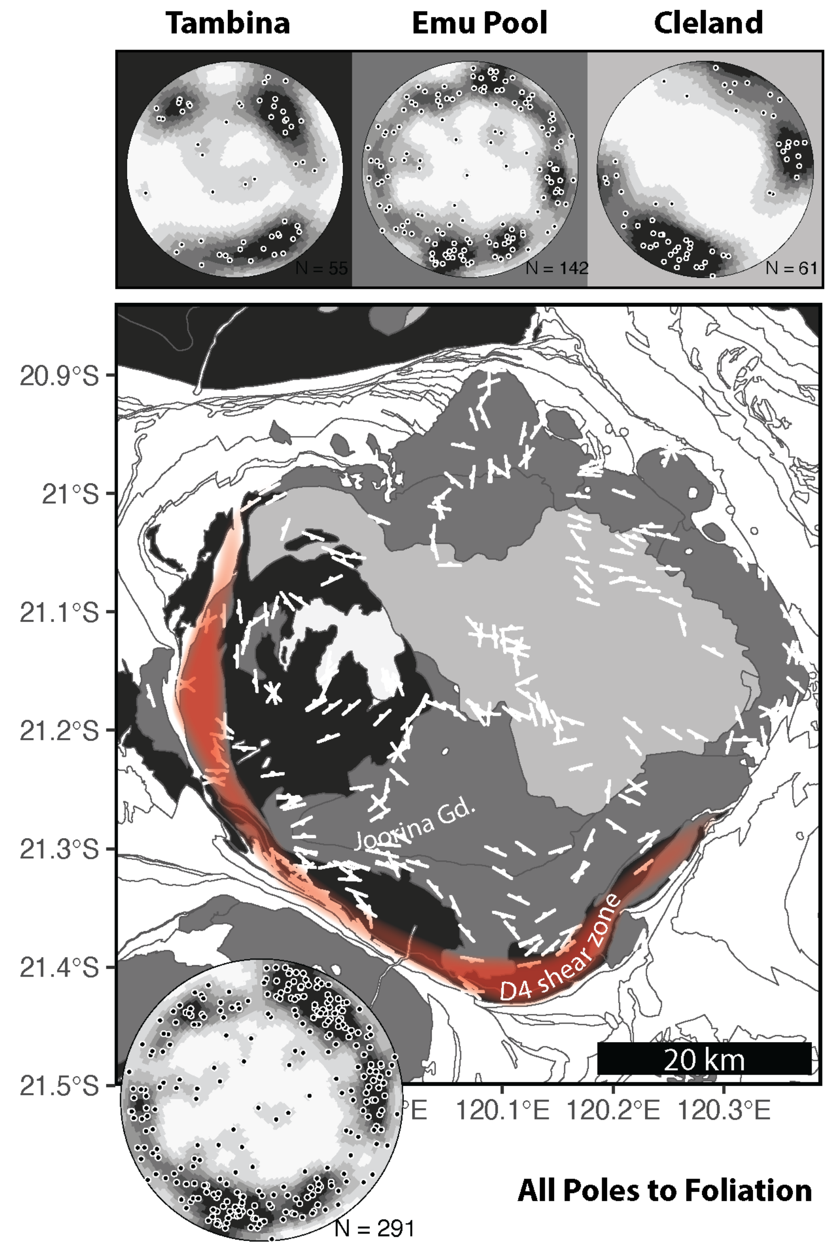

Figure 3. Geologic map and equal area nets with Kamb contours summarizing field measurements of foliations in granitic rocks of the Mt Edgar dome. The D4 shear zone of Collins (1989) is denoted by the red shaded region. Small equal area nets along the top of the figure have been separated out into supersuites, with the background corresponding to the map color. The large equal area net at the bottom right summarizes the entire dataset. Kamb contour intervals are σ = 3, 6, 9, 12, 15, 18.

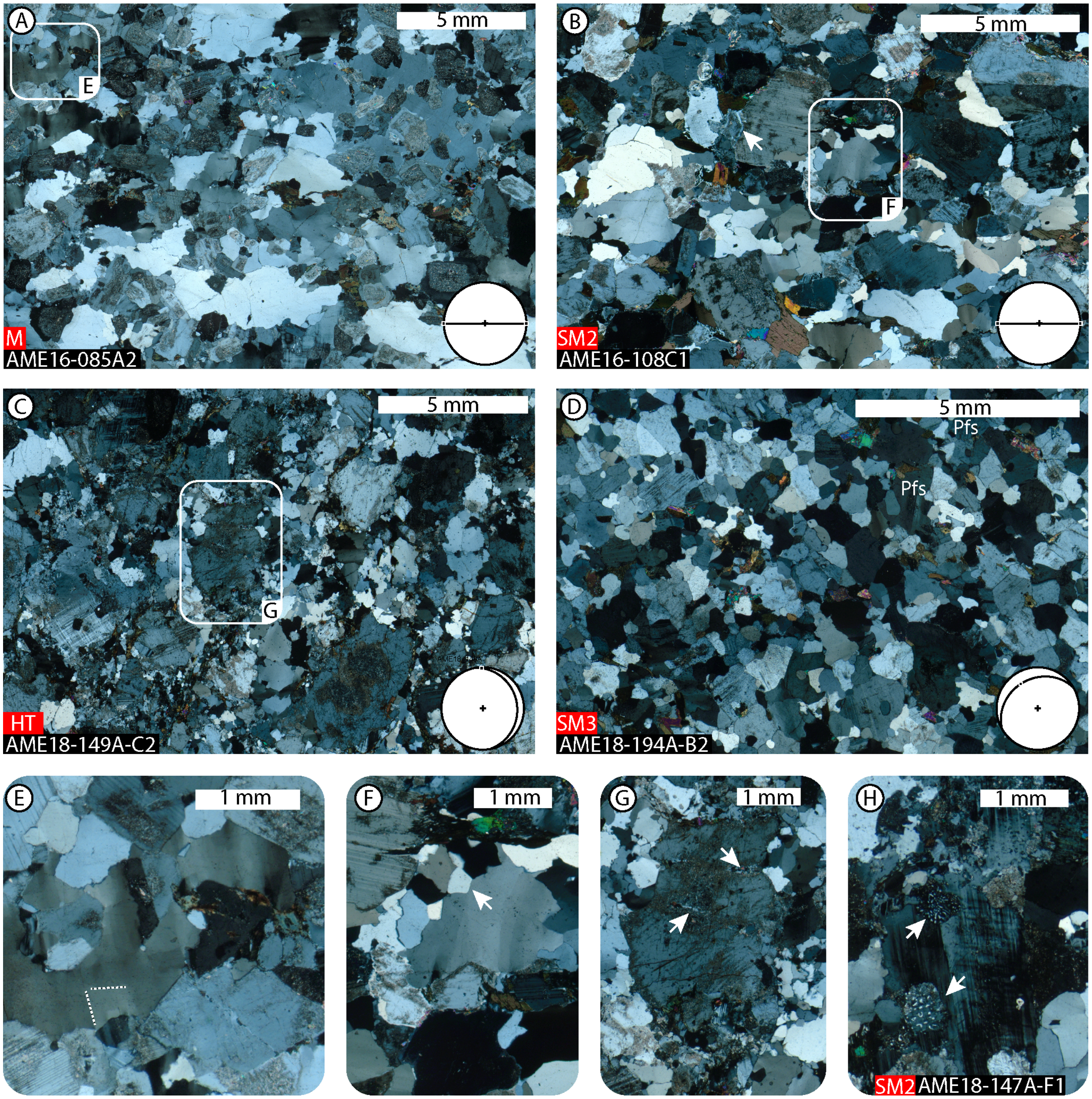

Figure 4. Representative microstructures from the rocks of the Bishop Creek Monzogranite Formation of the Cleland Supersuite. The location of each thin section is given on the map in Figure 7. A) An example of Magmatic microfabric. Small plagioclase laths (~1 mm length) appear randomly oriented in a matrix of large poikilitic alkali feldspar. Chessboard extinction in quartz is common (E). B) An example of Submagmatic fabric. Plagioclase laths are approximately aligned with foliation and have cuspate-lobate boundaries with quartz. Fractures in plagioclase is infilled with quartz (white arrow). A thin film of alkali feldspar rims many plagioclase laths, which is interpreted as evidence for melt presence. Quartz has a chessboard extinction, and in some places new grains have square boundaries that match the chessboard pattern (F). C) An example of a high temperature solid state microfabric. Quartz is more finely recrystallized than in (A) or (B), and feldspar is also finely recrystallized on sides of phenocrysts that are aligned with lineation. Feldspars that have infilled fractures provide evidence for an earlier submagmatic history. D) An example of a near-solidus Submagmatic fabric. Feldspars and quartz are both recrystallized into a polyphase aggregate of large grain size and amoeboidal grain boundaries.

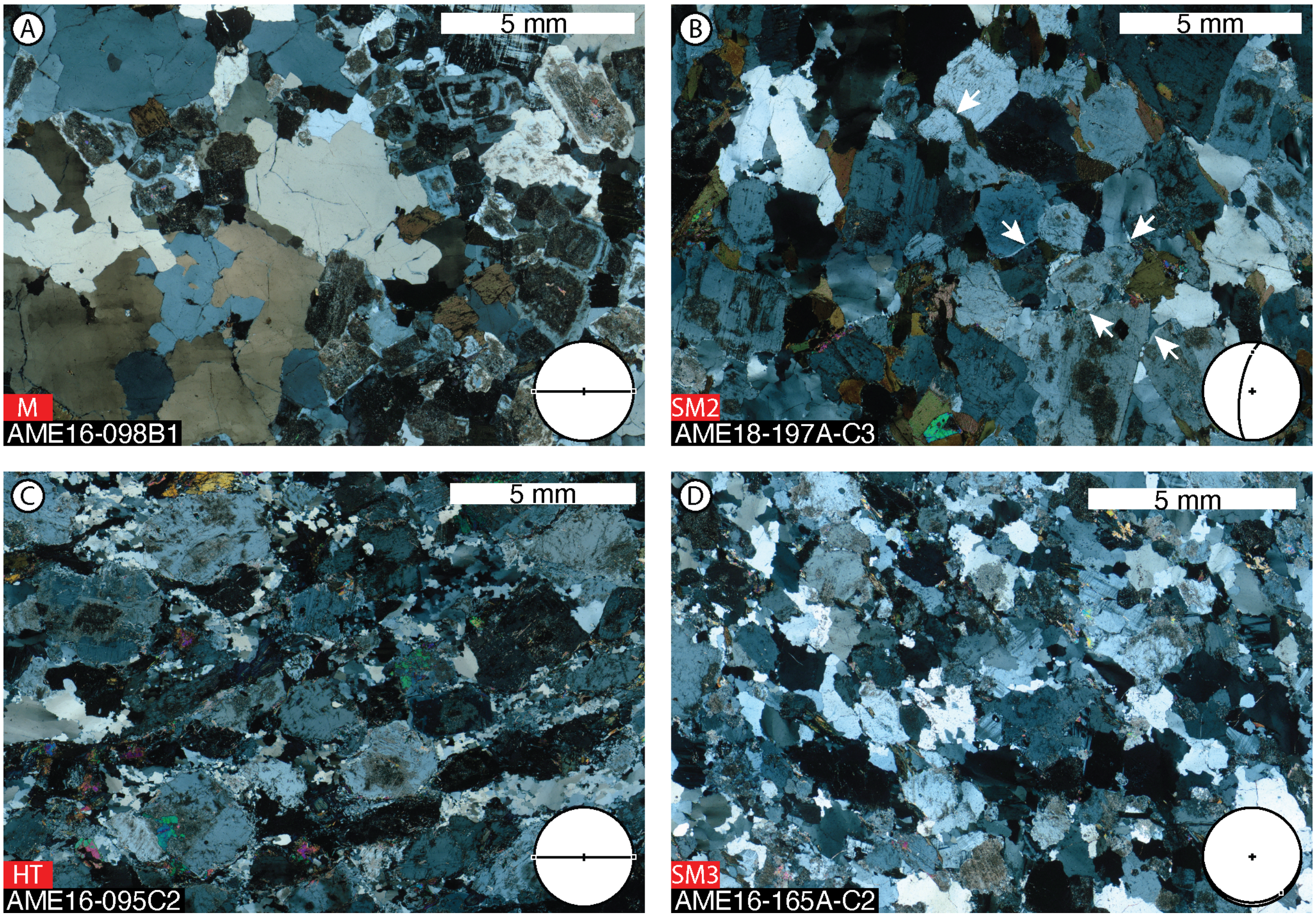

Figure 5. Representative microstructures for rocks belonging to the Emu Pool Supersuite. The location of each thin section is given on the map in Figure 7. A) Magmatic fabric, with randomly oriented Plagioclase, poikalitic microcline, and very large quartz grains exhibiting chessboard extinction. B) Submagmatic fabric, with infilled fractures in plagioclase (upper white arrow), partially recrystallized quartz, and a thin film of alkali feldspar lining many plagioclase laths (lower four white arrows). C) High temperature solid-state fabric defined by recrystallized quartz ribbons and rounded, partially recrystallized feldspars. D) Near-solidus submagmatic fabric defined by a polyphase aggregate of recrystallized quartz and feldspar.

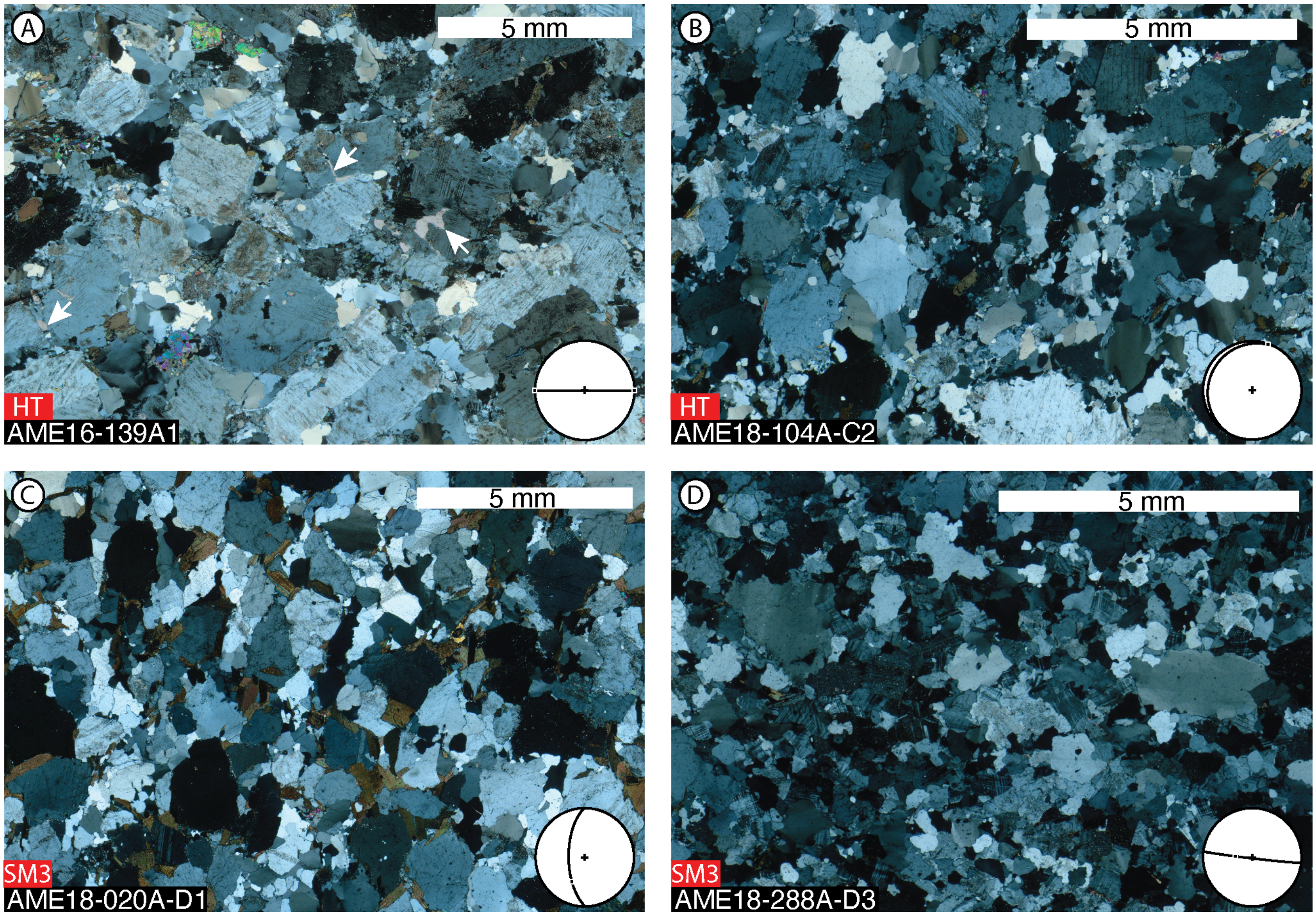

Figure 6. Representative microstructures of rocks within the Tambina Supersuite. The location of each thin section is given on the map in Figure 7. A) and B) High temperature solid state fabric defined by rounded, partially recrystallized feldspars separated by an anastamosing network of quartz ribbons. Recrystallized quartz grains are large with amoeboidal to polygonal grain boundaries. C and D) Example of near-solidus submagmatic microstructures. Quartz and feldspar are recrystallized and mix to form a polyphase aggregate.

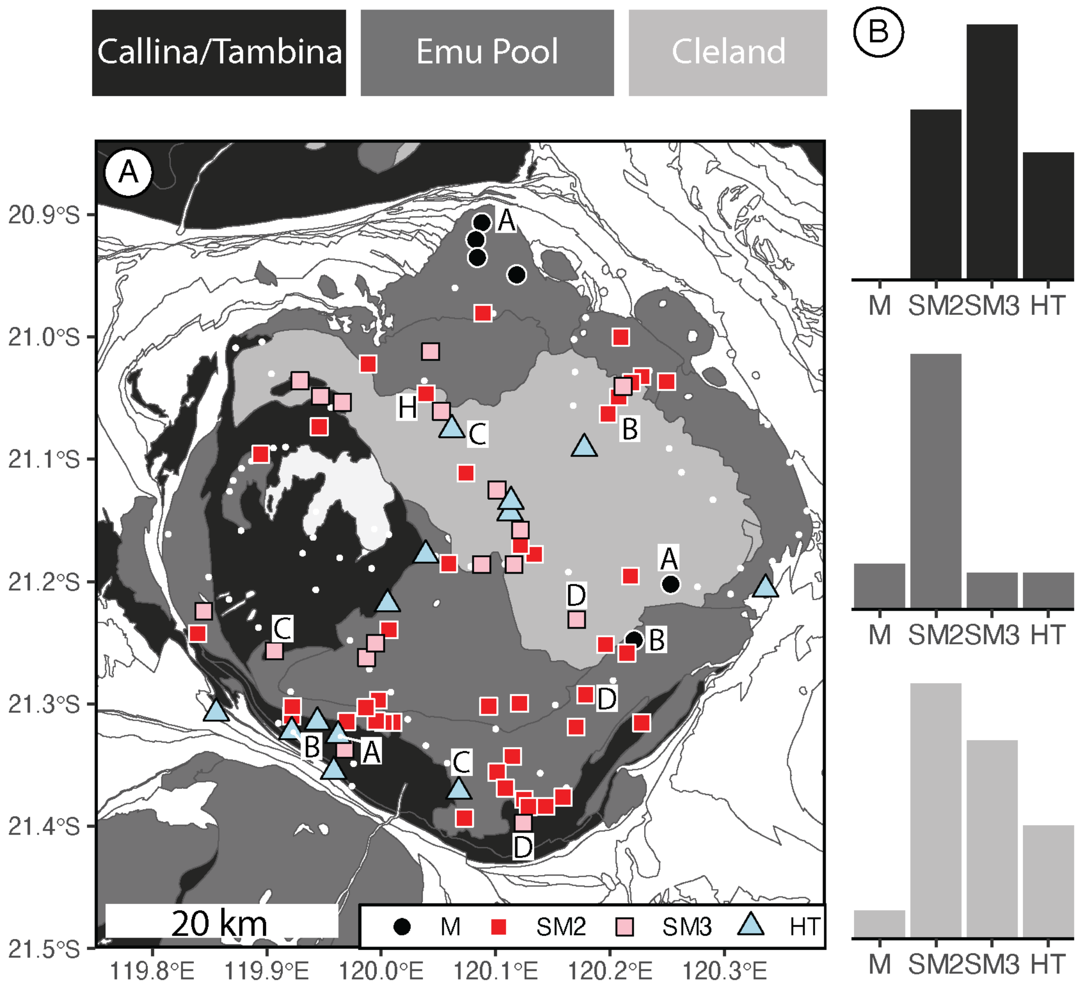

Figure 7. Summary of microstructural results. A) Distribution of microstructures in the Mt Edgar dome: M—Magmatic; SM2—Submagmatic Type II; SM3—Submagmatic Type III; HT—High temperature solid state. See text for descriptions. Microstructures were analyzed for more than half of AMS stations; small white dots represent the locations of AMS stations without microstructural characterization. B) Histograms representing the relative proportion of each microstructure type in each of the three main supersuites within the Mt Edgar dome. The grey of each histogram matches the grey of the mapped units.

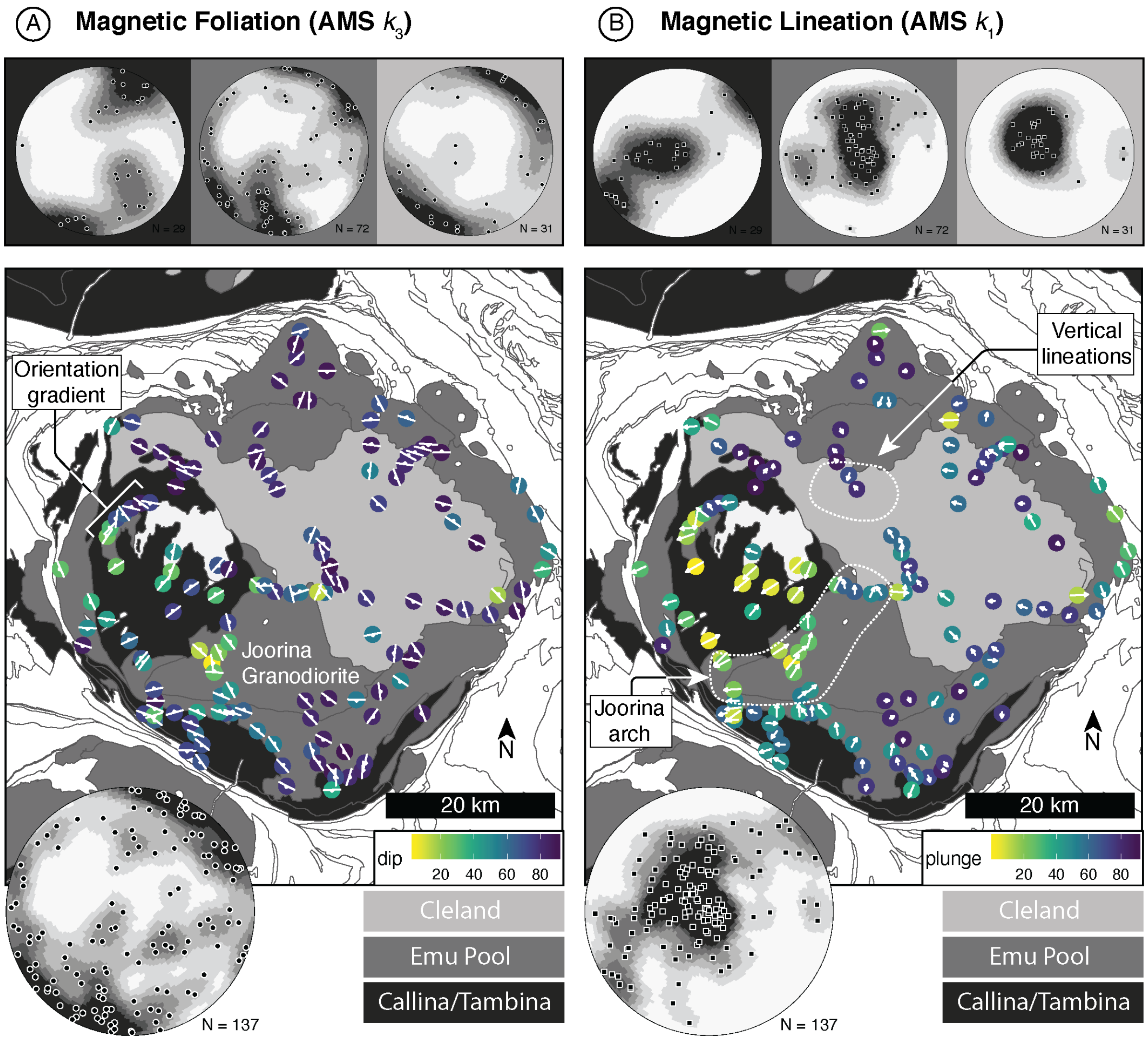

Figure 8. Summary of spatial distribution of interpreted foliation (A) and lineation (B) from mean AMS ellipsoids at each station. Equal area projections of poles to foliation and lineation are plotted with shaded Kamb contours. Kamb contours are $\sigma = 3{,}6{,}9{,}12{,}15{,}18$. Two structural features are annotated on the figure. Three geographic areas referred to in the text are highlighted: A region of closely spaced AMS data reveal a gradational change in orientation in panel A; Lineations within the Cleland and Emu Pool supersuites plunge radially inward toward a zone of vertical lineations in panel B; Lineations define a large scale arch from the center of the dome to the southwestern margin in panel B, which we refer to as the Joorina arch.

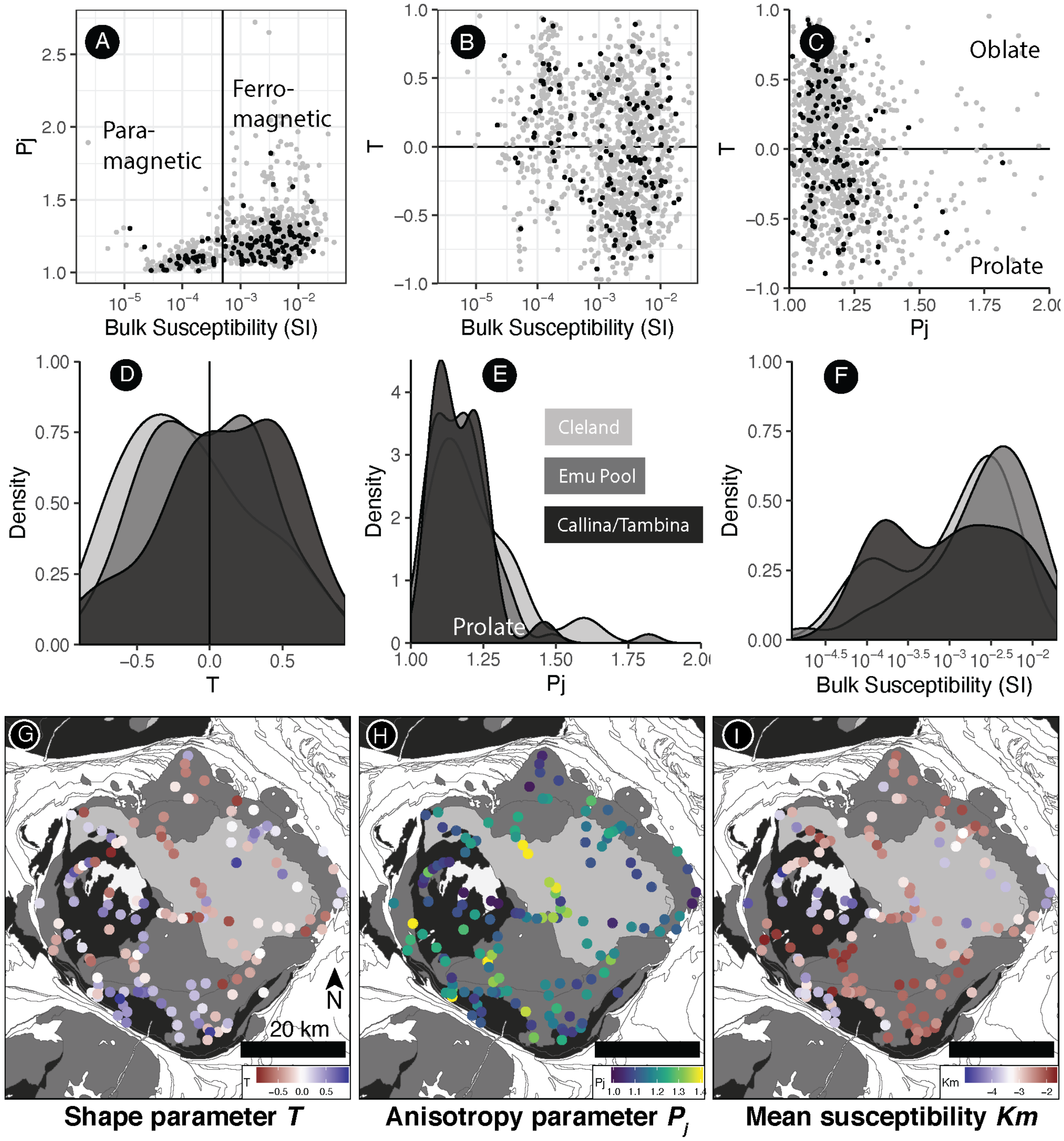

Figure 9. A summary of AMS parameter results. For A-C, grey points are individual core specimens, black points are station means. A) Bulk susceptibility versus anisotropy degree P_j shows that higher susceptibility samples have a wider range of anisotropies. B) Bulk susceptibility versus shape parameter T shows that lower susceptibility samples tend to have oblate shapes. C) Anisotropy degree versus shape parameter T shows that there is no strong dependency of shape on anisotropy degree. D) Probability density function plot of shape anisotropy P_j colored by supersuite. All supersuites have similar maxima, but Cleland supersuite has a larger spread than the other two. E) Probability density function plot of shape parameter T, colored by supersuite. Cleland rocks have a tendency toward prolate shape, Emu Pool rocks tends towards plane strain shape, and Tambina rocks tend towards oblate shape. F) Probability density function plot of bulk susceptibility, colored by supersuite. G) Shape parameter T. Blue colors represent oblate ellipsoids, white represents plane strain ellipsoids, and reds indicate prolate ellipsoids. H) Anisotropy parameter P_j. Blue color represents low anisotropy, yellow color indicates high anisotropy. I) Mean susceptibility. Blue color indicates low susceptibilities in the paramagnetic field, red color indicates high susceptibility in the ferromagnetic field. The scale is log(bulk

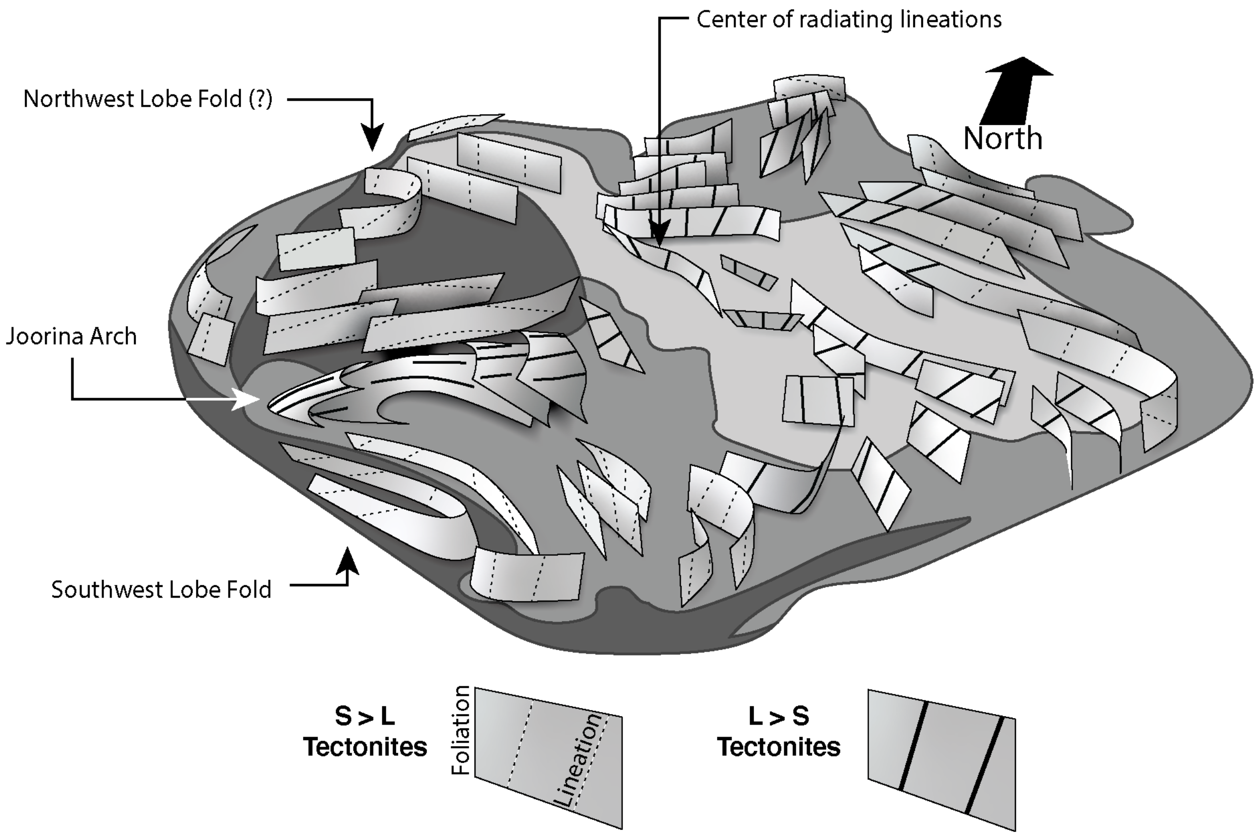

Figure 10. Illustration of the internal structure of the Mt Edgar dome, interpreted from AMS foliations and lineations. Four important features are: 1) The dome-wide, northwest-southeast striking, subvertical foliations with subvertical lineations; 2) Inward radiating lineations in the Cleland supersuite; 3) The Joorina arch that separates the two lobes of the Tambina supersuite; and 4) The Tambina is folded against the margin of the dome.

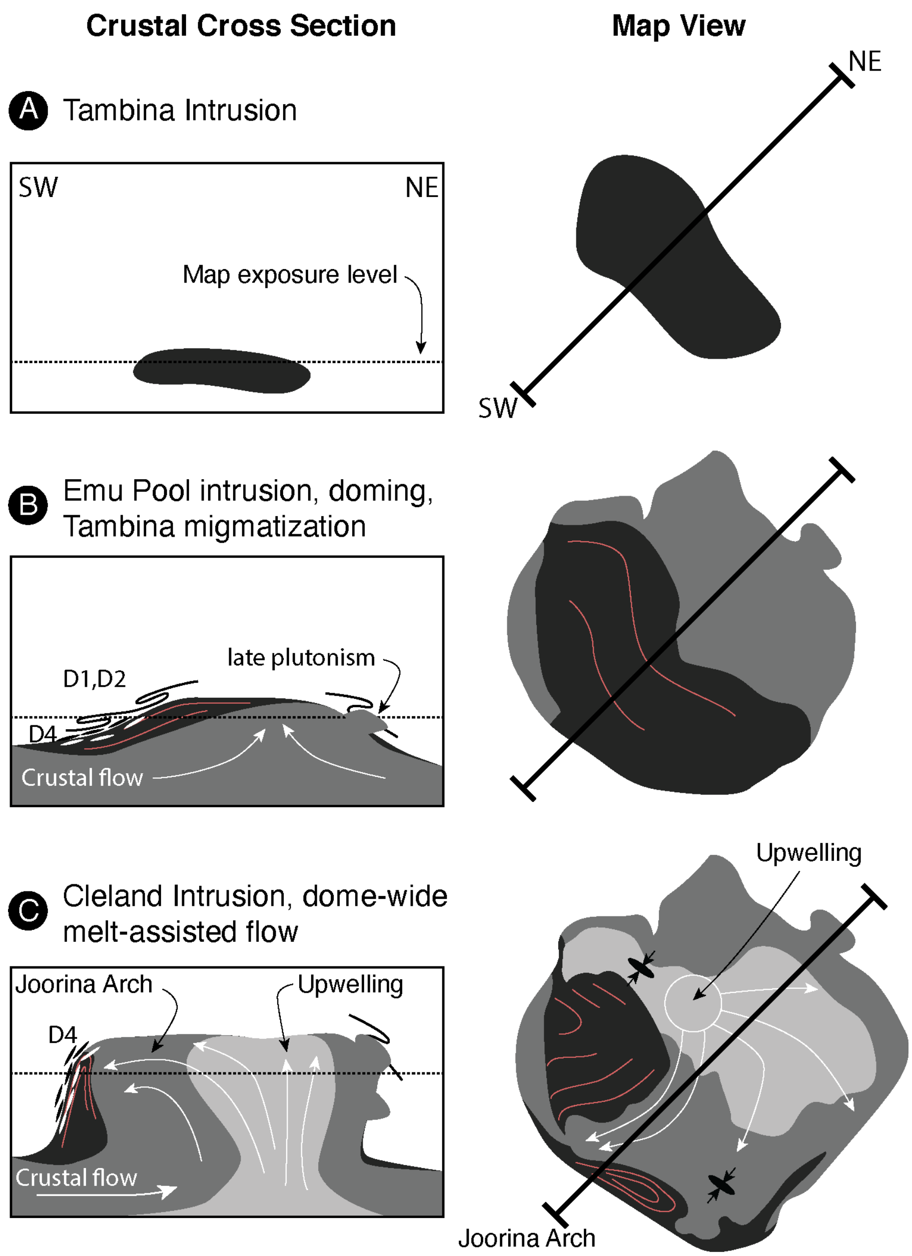

Figure 11. Three-step structural evolution of the Mt Edgar dome. A) Early Tambina Supersuite rocks intruded into basaltic crust between 3.47 and 3.42 Ga. B) Emu Pool magmatism is widespread, forming a granodioritic lower crust. Crustal flow focuses magmatism into deep crustal domes. Heating by younger units lead to extensive anatexis of Tambina Supersuite formations. Greenstone rocks are isoclinally folded as doming proceeds (D1 and D2 of Collins (1989)). Let in this doming process, Emu Pool plutons intrude the greentone belts to the north, and deformation localizes along Tambina Supersuite migmatites. This localization initializes the D4 shear zone of Collins (1989) C) Late Emu Pool and Cleland magmatism reheats older units and dome rocks rise into the upper crust. Emu Pool rocks fold and pinch Tambina rocks against the